Hindawi
Geofluids
Volume 2022, Article ID 8625005, 24 pages
https://doi.org/10.1155/2022/8625005

Research Article

Impacts of Sedimentation and Diagenesis on Deeply Buried Reservoir Quality of a Rift Basin: A Case Study of Wenchang Formation in the Lufeng Depression, Pearl River Mouth Basin, China

Panke Sun,[1] **Shiyi Jiang**,[1] **Lin Zhang**,[2] **Langbo Jia**,[3] **Huawen Rao**,[4] **Huijing Fang**,[5] **Zhen Yi**,[6] **Taihong He**,[2] **Sicheng Zhu**,[1] **and Liyin Bao**[1]

[1]*College of Geosciences, China University of Petroleum-Beijing, Beijing 102249, China*
[2]*CNPC Xibu Drilling Engineering Co., Ltd., Wushenqi 017300, China*
[3]*Research Institute of Exploration and Development, CNPC Changqing Oil Field, Xi'an 710000, China*
[4]*PetroChina Tarim Oilfield Company, Korla 841000, China*
[5]*Exploration Research Institute, Anhui Provincial Bureau of Coal Geology, Hefei 230000, China*
[6]*Shenzhen Branch of CNOOC Ltd., Shenzhen 518000, China*

Correspondence should be addressed to Panke Sun; sunpk@cup.edu.cn and Shiyi Jiang; jiangshiyicup@163.com

Received 11 May 2022; Revised 3 July 2022; Accepted 18 July 2022; Published 28 August 2022

Academic Editor: Dengke Liu

The deeply buried reservoirs of Wenchang Formation in the Lufeng Depression, Pearl River Mouth Basin, display strong heterogeneity, and the major controls for the development of high-quality reservoirs remain unclear. To address these issues, we conducted a series of experiment analyses, including petrographic microscope, scanning electron microscopy, and X-ray diffraction, and analyzed the impacts of sedimentation and diagenesis on the quality of deeply buried reservoirs. The results demonstrate that the sandbodies of subaqueous distributary channel and mouth bar deposited in lowstand systems tract (LST) and highstand systems tract (HST), as compared to the beach-bar and subaqueous fan sandstones deposited in transgressive systems tract (TST), have coarser grain size, higher quartz content, and lower muddy matrix content, which induced stronger anti-compaction capability, higher preservation of intergranular pore spaces, and thus better reservoir qualities. The reservoir types developed in subaqueous distributary channel and mouth bar are mainly types I, II, and III with medium-low porosity and low-ultra low permeability, while beach-bar and subaqueous fan mainly developed type III reservoir with low-porosity and ultra-low permeability. The reservoirs developed in E_2w of the study area have undergone strong compaction, intense dissolution, but weak cementation. The subaqueous distributary channel and mouth bar reservoirs in LST are adjacent to Ew_4 source rock in spatial distribution, resulting in strong organic acid dissolution, and developed numerous dissolved pores. The charging of hydrocarbons before deep burial further inhibited the later compaction and cementation and protects the preservation of residual primary intergranular pores and secondary dissolved pores. The combination of these factors leads to the development of the abnormally high porosity and high-quality reservoirs in LST. The results of this study reveal the genetic mechanism of deep, high-quality reservoirs in the rift basin and guide the selection of high-quality reservoirs in the later stage.

1. Introduction

With the enhancing exploration degree of mid-shallow reservoirs, most oil and gas resources have been discovered, and the future oil and gas exploration targets will be expanded to deep sea and deep earth [1–6]. However, as compared with shallow buried reservoirs, deep buried reservoirs have experienced complex geological processes; thus, the influencing factors of reservoir quality are also more complicated, including sedimentation under the constrain

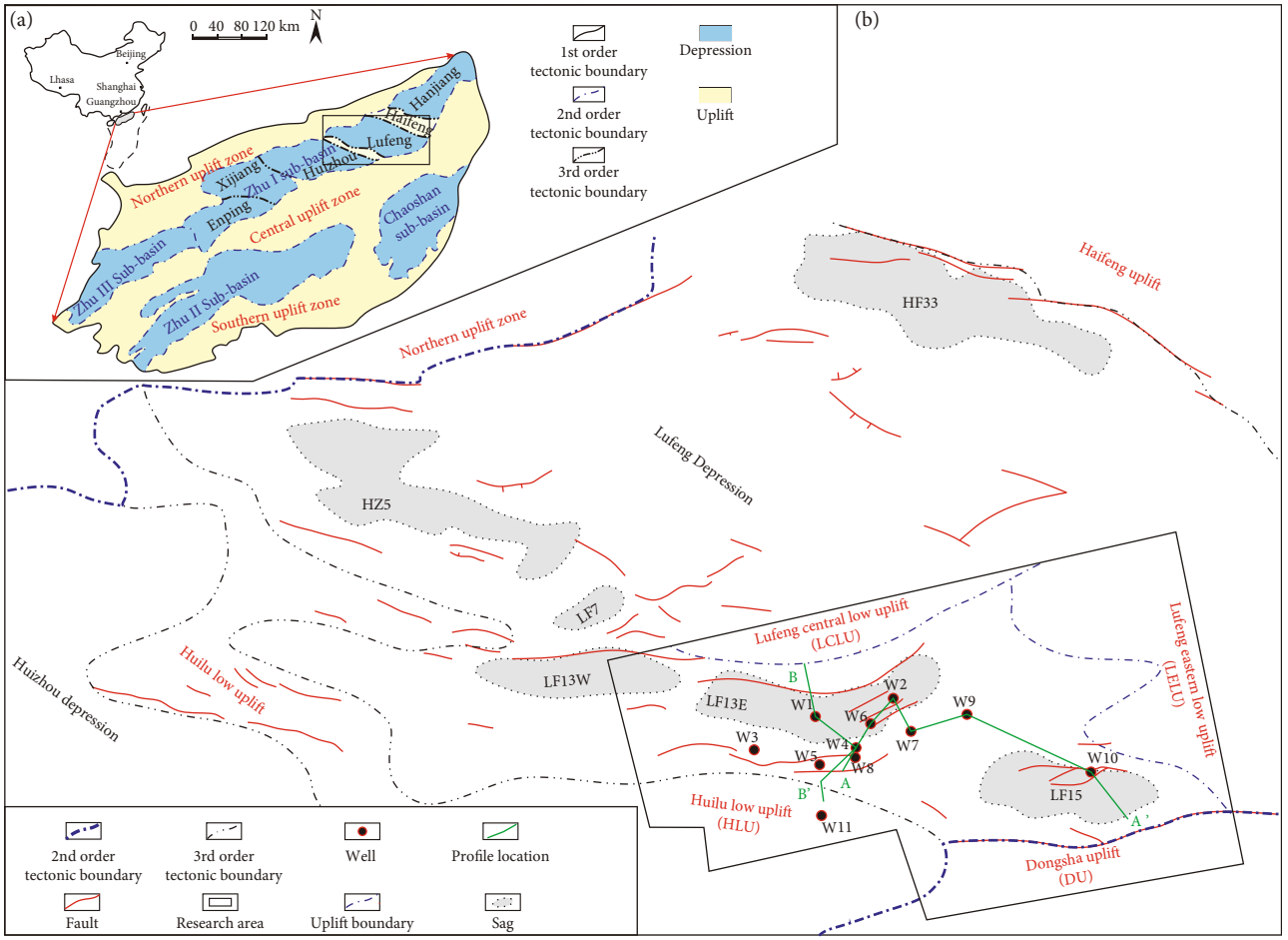

FIGURE 1: (a) Location of the Lufeng depression in the Pearl River Mouth Basin of China. (b) Location of the research area in the Lufeng depression.

of sequence framework, diagenesis, tectonic movement, burial patterns, abnormal overpressure, and hydrocarbon charging [7–19]. The change of sea level will lead to the development of different sequence types and sedimentary facies types. Reservoirs in different facies types have different material compositions, such as mineral composition, particle size, and sorting, which will lead to different characteristics of the original pore structure of the reservoir, and then affect the later diagenesis [8, 13, 14, 20–23]. For this reason, linking diagenetic processes and diagenetic evolution to their corresponding sequence types and sedimentary facies types can trace the source, which provides an effective means for diagenetic evolution analysis and reservoir heterogeneity prediction [10, 13, 24–26]. Diagenesis is a process of changing the original reservoir characteristics, including porosity, pore structure, and permeability. Mechanical compaction and chemical compaction can change the size, distribution, and connectivity of original pores and pore throats [27–30]. With the increase of burial depth, compaction and cementation can further reduce the primal porosity and permeability, but the secondary pores formed by mineral dissolution can also greatly improve the quality of deeply buried reservoirs [31–35].

For rift basins, the development of sequence units and sedimentary facies in the basin is complex and diverse due to the complexity of basin tectonic movements and the diversity of provenance systems [36–38]. For example, in the early stage of Paleogene rifting, the Qiongdongnan Basin mainly developed lowstand systems tract and deposited alluvial fans and braided rivers. However, in the middle-late stages of rifting, three-divided system tracts are well developed, and sedimentary facies types, such as braided river delta, fan delta, nearshore subaqueous fan and submarine fan, are all diversely developed [39]. Under the influence of tectonic movement, the sediments deposited in rift basin will undergo a complex diagenetic evolution process, and the diagenetic evolution time and processes of deeply buried reservoirs will be longer and more complex as compared with shallow buried reservoirs [40–42]. For this reason, the quality of deeply buried reservoirs is generally considered to be relatively poor. With the enhancing exploration degree, more high-quality reservoirs are discovered in deep earth. For example, the buried depth of the Lower Cretaceous Tuscaloosa Formation in Gulf of Mexico Basin reaches 6600 m, but the reservoir porosity and permeability can still reach 26% and 72 mD [43]. Therefore, different from our previous

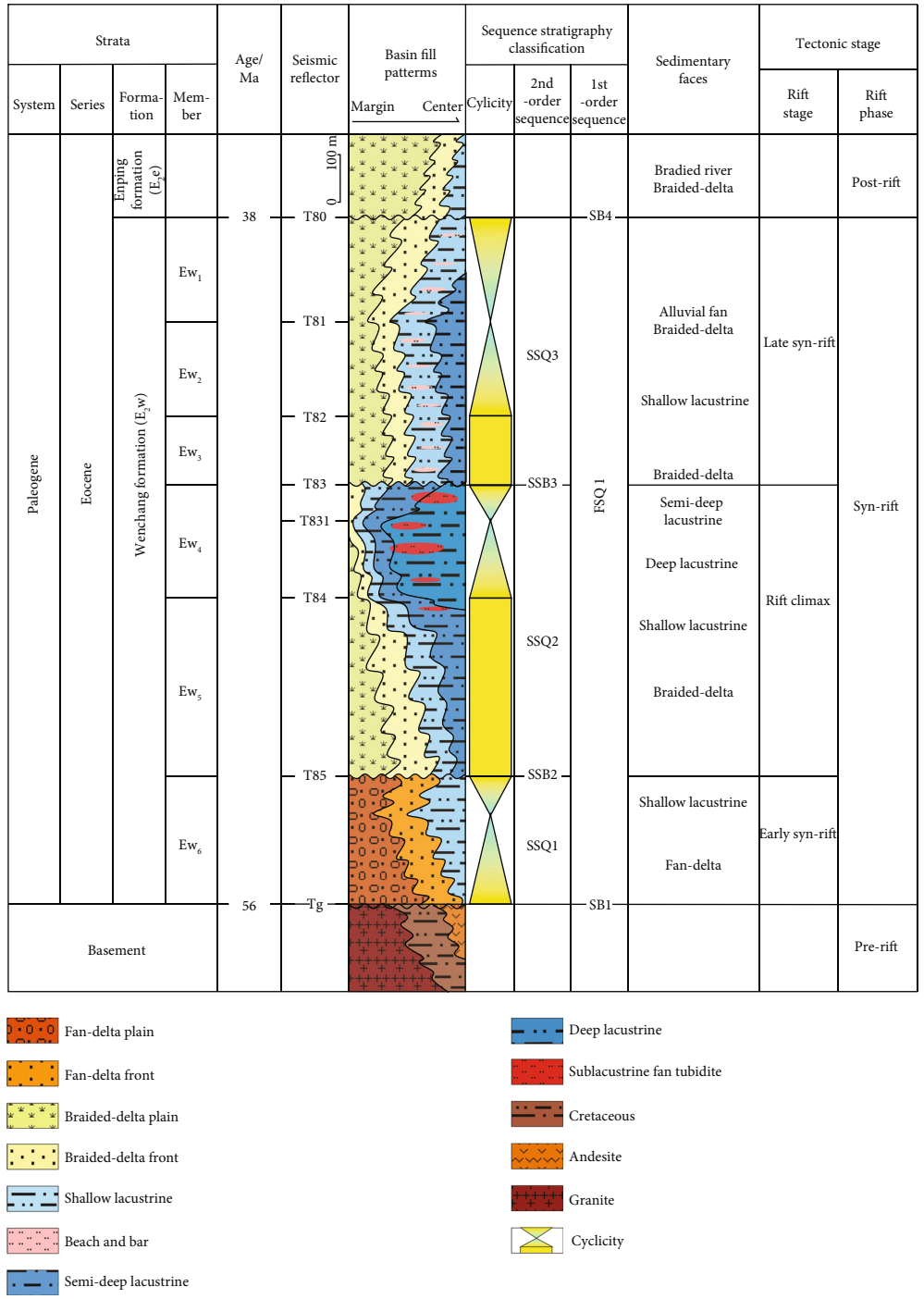

Figure 2: Sequence stratigraphy characteristics of the Eocene Wenchang Formation in Pearl River Mouth Basin (modified from [36]).

understanding, deeply buried reservoirs still have great exploration potential. In view of this, China's oil and gas exploration has gradually shifted to deep and ultra-deep strata and even made breakthroughs in strata greater than 8000 m in recent years. However, the genetic mechanism of such high-quality reservoir needs to be further studied. Various factors such as early shallow burial and late rapid deep burial, early compaction, and late dissolution can all lead to the development of high-quality reservoirs [8, 44–46], and the genetic mechanisms in different regions are also different. The reservoir of Wenchang Formation in Lufeng Sag, Pearl River Mouth Basin, has the characteristics of deep burial, complex sedimentary environment changes, various types of sedimentary facies, and complex diagenesis and evolution. The control factors for the development of high-quality reservoirs and the distribution law of favorable reservoirs are not clear. Therefore, the research on the impacts of sedimentation and diagenesis on reservoir quality can not only supplement the genetic mechanism of deeply buried reservoirs with high quality in the rift basin but also establish

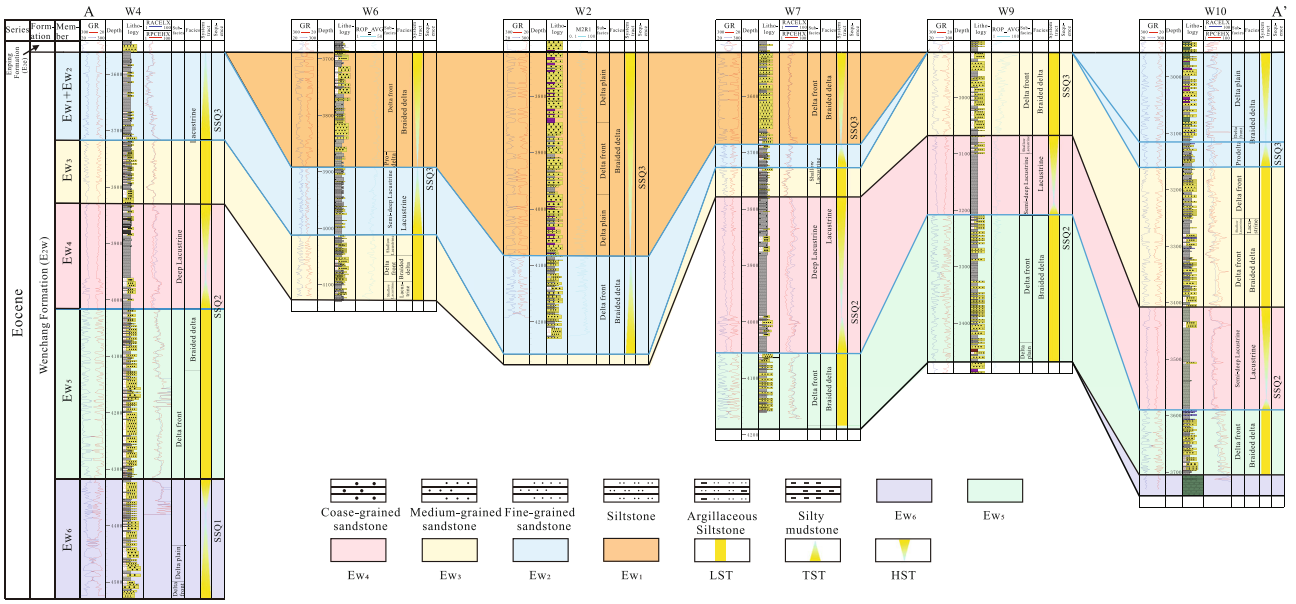

FIGURE 3: Regional stratigraphic correlation profile AA' of E_2w, and the location of the profile AA' is given in Figure 1(b). The different colors represent different members of E_2w. It also shows the sequence classification and depositional facies according to the logging facies and lithological association.

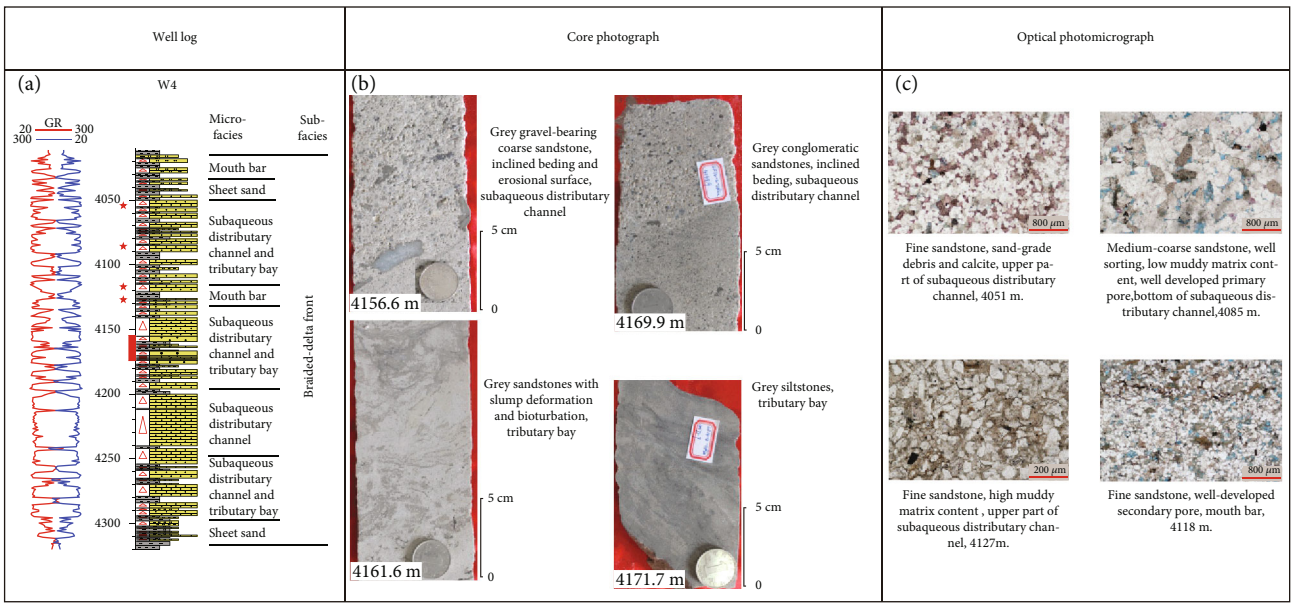

FIGURE 4: Typical logging curves (a), core photos (b), and optical photomicrograph (c) show the braided-delta front characteristics, especially the subaqueous distributary channels and mouth bar. The well location is marked in Figure 1.

the foundation for the prediction of favorable reservoirs in the study area.

2. Geological Setting

2.1. Tectonic Setting. The Pearl River Mouth Basin, located in the eastern part of the northern margin of the South China Sea (Figure 1(a)), is a passive continental margin rift basin formed in the Cenozoic with a total area of 17,500 km^2 [47, 48]. The Zhu I sub-basin is located in the northeastern part of the Pearl River Mouth Basin with a NE-SW trending and covers an area of 7,750km^2 [49, 50]. The Zhu I sub-basin is composed of Enping, Xijiang, Huizhou, Lufeng, and Hanjiang depressions from west to east (Figure 1(b)). Lufeng depression, surrounded by Northern Uplift Zone, Huilu Low Uplift (HLU), Dongsha Uplift (DU), and Haifeng Uplift, contains five sags including HF33, HZ5, LF7, LF13W, LF13E, and LF15. The study area, located in the southern Lufeng depression, includes LF 13E sag and LF 15 sag with an area of 2,100 km^2. The tectonic

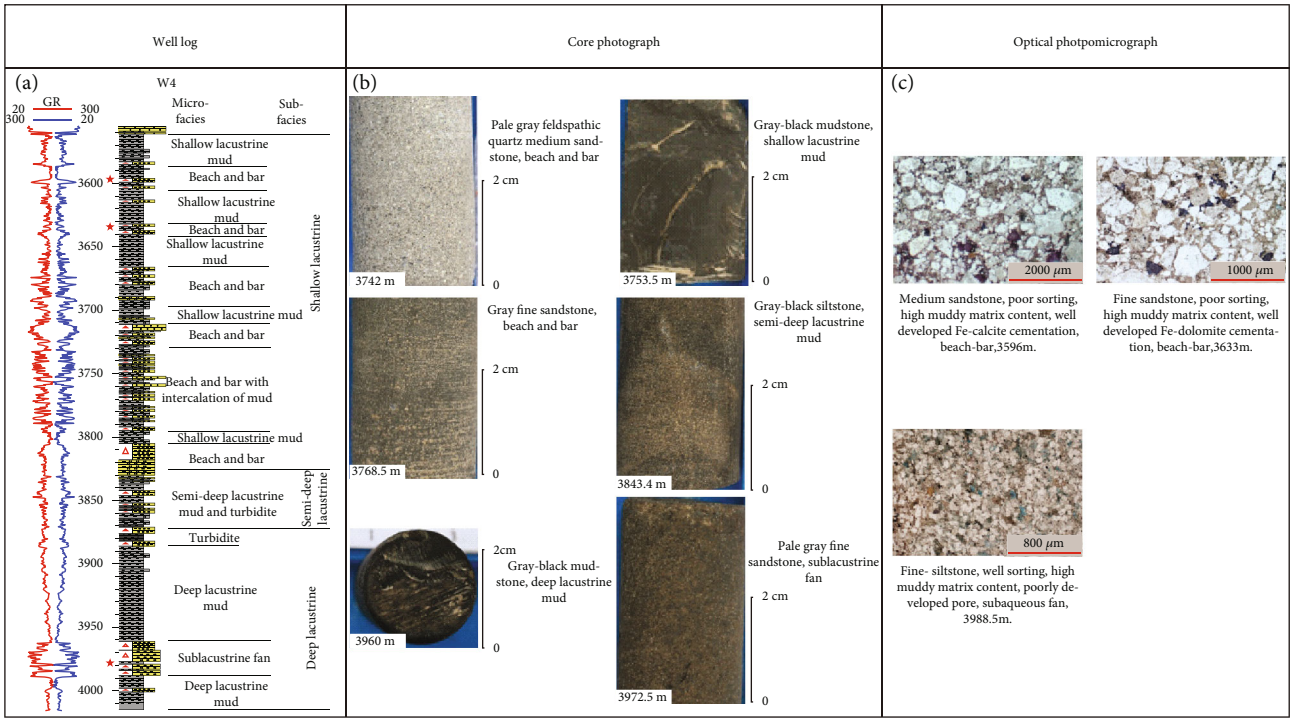

FIGURE 5: Typical logging curves (a), core photos (b), and optical photomicrograph (c) show the Lacustrine characteristics, especially the beach-bar and subaqueous fan. The well location is marked in Figure 1.

evolution of Lufeng depression can be divided into two phases, the syn-rift phase and the post-rift phase. From the bottom up, the Wenchang Formation (E_2w) and Enping Formation (E_2e) correspond to the syn-rift phase and post-rift phase, respectively [51]. Furthermore, based on the evidence of tectonic activities, unconformities, and sedimentary cycles, the syn-rift phase of the deposition of E_2w can be further subdivided into three typical stages: the early syn-rift (Ew_6), the rift climax (from Ew_5-Ew_4), and the late syn-rift (from Ew_3-Ew_1) [36].

2.2. Sequence and Sedimentary Characteristics. The Wenchang Formation mainly deposited terrestrial sediments and can be divided into six members (Ew_6-Ew_1) from the bottom up based on lithological differences and sedimentary cycles. According to the characteristics of well logs and seismic reflection of the interfaces within E_2w, two first-order sequence boundaries (SB1 and SB4) and two second-order sequence boundaries (SSB2 and SSB3) were identified (Figures 2 and 3). Based on the identified sequence boundaries, the rift-related Wenchang Formation can be further divided into one first-order sequence (E_2w) and three second-order sequences, including SSQ1, SSQ2, and SSQ3, which correspond to the early syn-rift phase (Ew_6), rift climax phase (Ew_5-Ew_4), and late syn-rift phase (Ew_3-Ew_1) [36]. SSQ1 is composed of transgressive systems tract (TST) and highstand systems tract (HST). SSQ2 is composed of lowstand systems tract (LST), TST, and HST. The LST corresponds to Ew_5, while the TST and HST correspond to Ew_4. SSQ3 is also composed of LST, TST, and HST and these system tracts correspond to Ew_3, Ew_2, and Ew_1, respectively.

According to the core description, thin-section analysis, shape of logging curve, and seismic reflect patterns, as well as papers published about the study area [3, 36], four main sedimentary facies were recognized in the study area: braided-delta facies, lacustrine facies, fan-delta facies, and nearshore subaqueous fan facies (Figures 4–6), which can be further divided into a variety of subfacies and microfacies. Three subfacies developed in braided-delta facies: braided-delta plain, braided-delta front, and predelta facies, and the sandbodies of braided-delta front are the main focus of this study. In braided-delta front facies reservoirs, the subaqueous distributary channel sandbodies mostly develop gravel sandstone or medium-coarse sandstone with positive rhythm and erosion surface, which are characterized by box, bell, or superimposed box and bell shapes in the GR log (Figure 4). The mouth bar sandbodies mostly develop relatively pure, cross-bedded medium-fine sandstone and the logging curves are funnel-shaped geometry. Sheet sand displays thin sandbodies interbedded with thin mudstone and has a finger-shaped log curve (Figure 4). The seismic reflections of medium amplitude, medium frequency, medium continuity, and sigmoidal or oblique clinoform indicate the braided-delta front deposits (Figure 6). The lacustrine is composed of shallow lacustrine and deep lacustrine, and the beach-bar and subaqueous fan are the two main sandbodies in this deposition environment. The beach-bar sandbodies, developed in shallow lacustrine facies, usually display thin interbedded medium-fine grained sandstones with mudstones, and the logging curves show a finger-shaped geometric structure. The subaqueous fan deposits in the deep lacustrine facies mostly develop thin medium-fine sandstone layers interposed in thick gray-

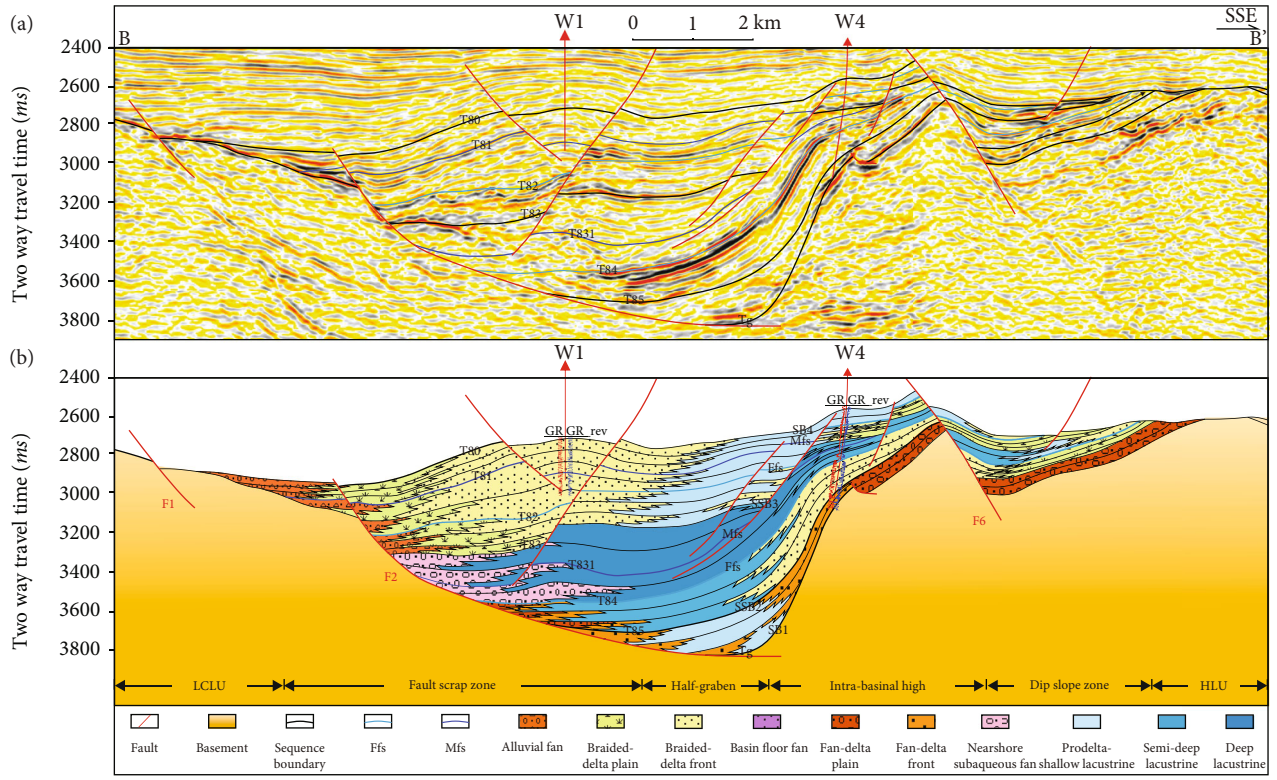

FIGURE 6: Profiles (crossing W1 and W4) in the central part of LF13E. (a) Seismic profile interpretation of faults and horizons. (b) Interpretation of depositional systems based on well and seismic reflection data. Location of profile BB' is marked in Figure 1(b) (modified from [37]).

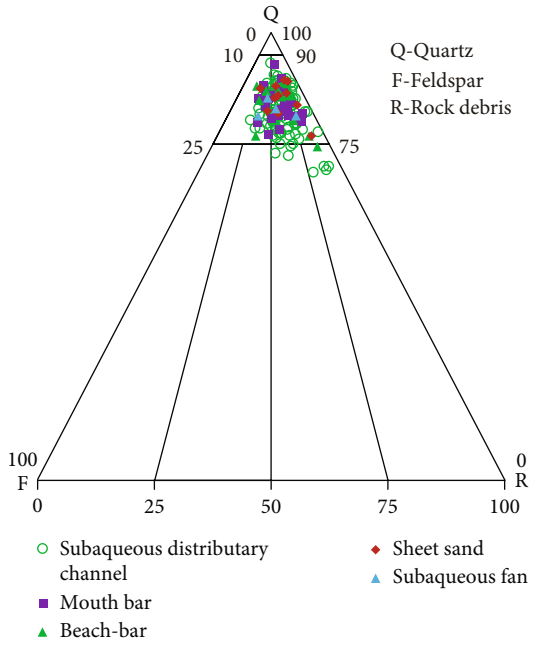

FIGURE 7: Detrital composition of sandstones of different microfacies in E_2w (ternary plot refers to the sandstone classification standard of Folk [55]).

black mudstone, and the logging curves are sawtooth features (Figure 5). In seismic profiles, shallow lacustrine facies display a chaotic sheet character, semi-deep lacustrine facies show high continuity parallel sheet seismic reflections, and deep lacustrine facies demonstrate semi-parallel sheet seismic reflections (Figure 6). Few wells have drilled fan-delta and nearshore subaqueous fan systems, but on the seismic profiles, fan-delta facies display the chaotic wedge-shaped or the progradational wedge-shaped reflection, whereas nearshore subaqueous fan systems typically show a chaotic wedge-shaped seismic reflection characteristic (Figure 6; [38, 52]). In general, the Wenchang formation experienced a sedimentary evolution of fan-delta – braided-delta – lacustrine – braided delta.

3. Materials and Methods

3.1. Materials. In this study, we collected 183 core samples and well-wall core samples in the reservoir intervals of the Wenchang Formation from 8 wells. All of these wells penetrated E_2w of the southern Lufeng depression. The depth of E_2w ranges from 2,900 m to 4,500 m.

3.2. Methods. The samples were analyzed and measured through a series of technics, including thin-section observation, scanning electron microscopy (SEM), X-ray diffraction (XRD), standard petrophysical helium porosity and air permeability, and organic matter of vitrinite reflectance analysis. All these experimental projects were completed at the Shenzhen Experimental Center of CNOOC Experimental Center, Engineering Technology Branch of CNOOC Energy Development Co., Ltd.

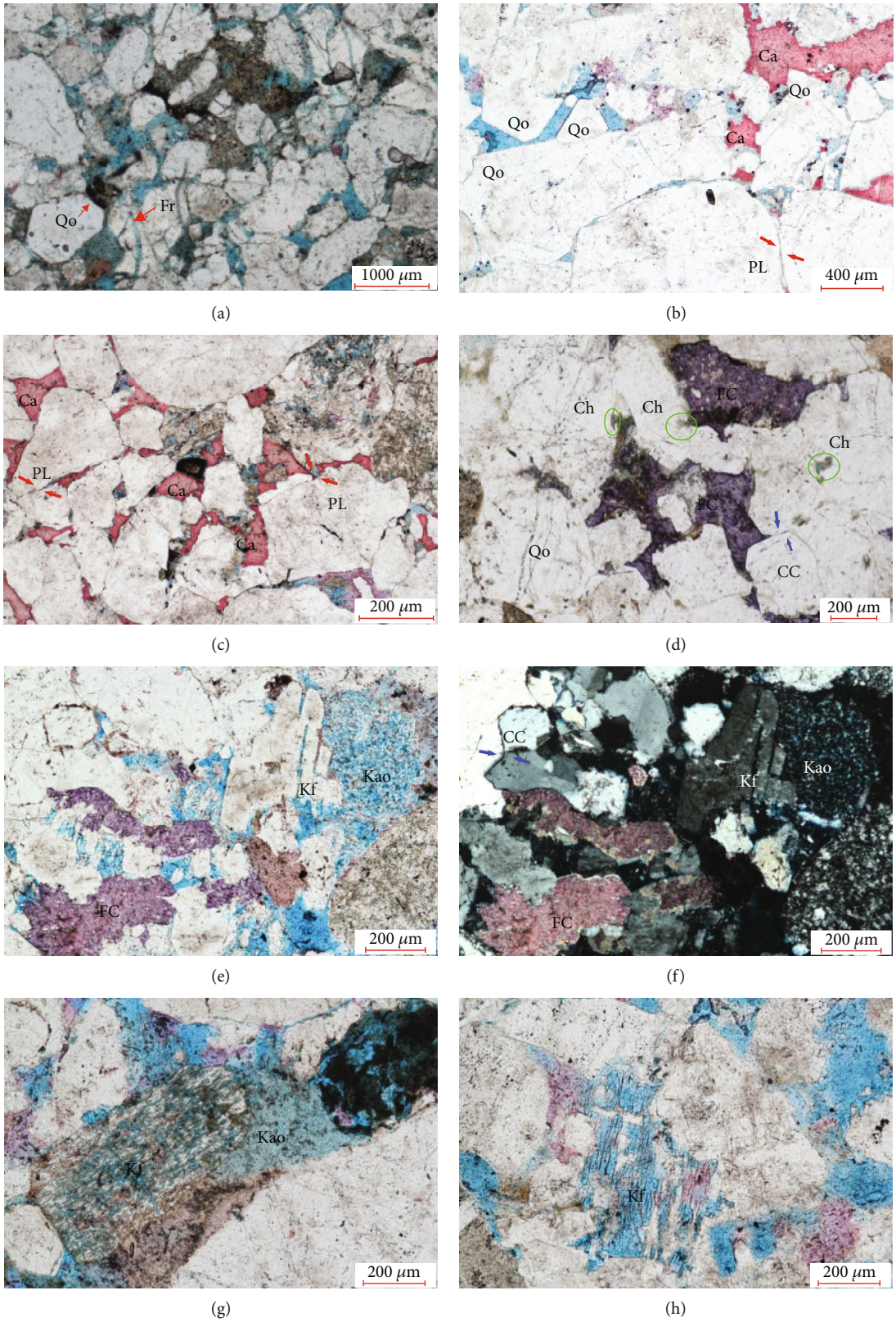

Figure 8: Continued.

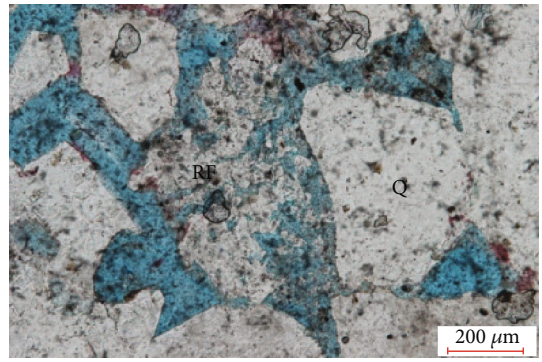

(i)

Figure 8: The diagenetic characteristics of E_2w in the southern Lufeng depression. (a) Debris particles are broken, and the edges of the particles show weak quartz overgrowth, 3701 m, W6. (b) Intergranular pores are filled with quartz overgrowth and early calcite cement, 4170.98 m, W4. (c) Intergranular pores are filled with early calcite cement, 4158.75 m, W4. (d) Residual intergranular pores are filled with Fe-calcite and chlorite cements, 4060.3 m, W7. (e) Residual intergranular pores are filled with Fe-calcite cement, the thin section also shows the intragranular dissolved pores in feldspar, 4190 m, W2. (f) The same characteristics of (e) in the orthogonal polarization, 4190 m, W2. (g) Feldspar is dissolved to form the dissolved pores, and the kaolinite is filled into the intergranular pores, 3611.4 m, W10. (h) The feldspar is completely dissolved, and the dissolved pores do not collapse. (i) The dissolution of the rock fragment, 3719.5 m, W6. Qo: quartz overgrowth; Fr: fracture; Ca: calcite; FC: Fe-calcite; Kf: K-feldspar; Kao: kaolinite; RF: rock feldspar; Ch: chlorite; PL: point-line contact; CC: concave-convex contact.

3.2.1. Petrographic Microscope. 183 thin sections were colored by epoxy resin and analyzed by a petrographic microscope. The amounts of detrital and diagenetic components, grain size, and the pore types and pore structure were determined by points counting (300 points in each thin section). Thin sections cover the main sedimentary microfacies in the study area. The carbonate cements were marked with an acid solution of alizarin red and potassium ferrocyanide for identification purpose [53].

3.2.2. Physical Properties Testing. 132 horizontal plugs were conducted standard petrophysical helium porosity and air permeability testing using Ultrapore-300 and KSY-1 equipment. These samples and partial studied thin sections correspond to each other.

3.2.3. Scanning Electron Microscope. 86 polished thin sections were prepared for SEM observation to study and distinguish clay minerals. The morphology and textural relationships among minerals were observed by a Quanta 200 scanning electron microscope equipped with an SEM detector.

3.2.4. X-Ray Diffraction. X-ray diffraction (XRD) analyses of the $<2\,\mu$m fractions were performed using the centrifuge method in a D/max-2500PC diffractometer in 125 samples [54].

3.2.5. Burial History and Thermal Evolution History. Burial history and source rock maturity history of E_2w in the study area were studied using BasinMoD software. The stratigraphic data of W7 were input into the software, and 26 vitrinite reflectance (Ro) data from 3 wells were used to constrain the paleotemperature of the stratum. Finally, the burial history and the thermal evolution history of the study area were established.

4. Results

4.1. Detrital Composition and Rock Fabric Characteristics. The lithology of sandstone in Wenchang Formation is primarily conglomerate, conglomeratic sandstone, medium-coarse sandstone, fine sandstone, siltstone, and heterogeneous sandstone (Figures 4 and 5). The conglomerate is mainly fine gravel, and the composition is simple and primarily composed of polycrystalline. The structure of the conglomerate is from sub-angular to sub-circular. The types of sandstone are mainly composed of lithic quartz sandstone with a little part of feldspar quartz sandstone (Figure 7). The average content of the detrital minerals is $Q_{82.7}F_{6.3}R_{11}$. Quartz includes single-crystal quartz (62.7%) and polycrystalline quartz (20%), the feldspar is dominated by K-feldspar (6% on average), and the lithic fragment is mainly the volcanic rock lithic fragment (8.1% on average), with a very small amount of the schist, mudstone, sandstone, and granite lithic fragments. The sorting of the sandstone is medium to poor and the rounding of sandstone is mainly from sub-circular to sub-angular. Mica is occasionally developed (most samples <1%). The matrix is primarily mudstone, with a content of 1%-19% (4.6% on average).

The detrital compositions of different sedimentary facies are basically the same (Figure 7), but the lithology is slightly different. The lithology of the subaqueous distributary channel is mainly the conglomeratic sandstone, medium-coarse sandstone, and heterogeneous sandstone. The lithology of the mouth bar, sheet sand, beach-bar, and the subaqueous fan is primarily the fine sandstone and siltstone. Among them, the mud content of the subaqueous distributary channel is the lowest (3.8% on average), the mouth bar and sheet sand are slightly low (5.9% and 5.5% on average, respectively), and the beach-bar and the subaqueous fan are a little high with an average content being 7.7% and 7.3%, respectively.

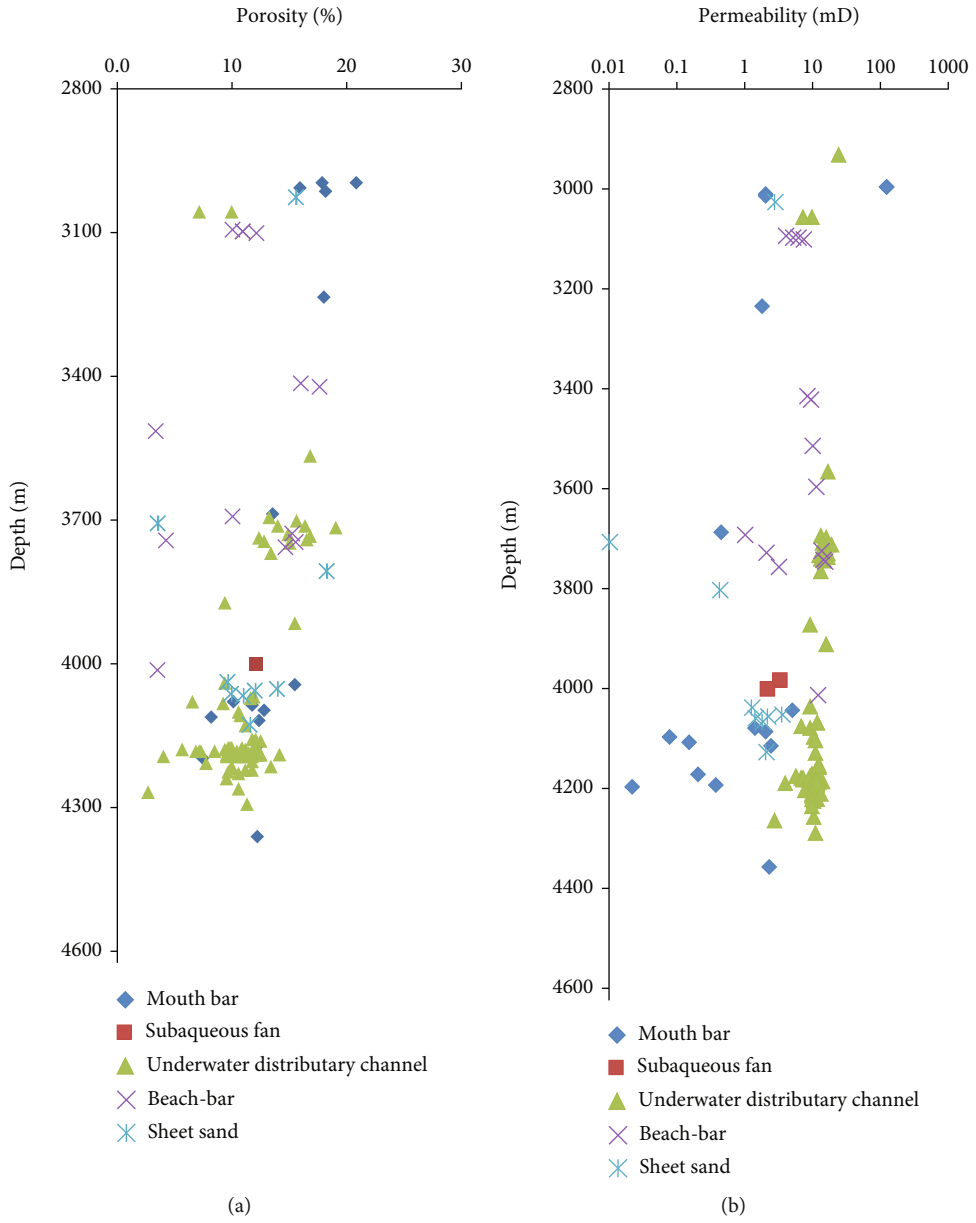

Figure 9: The vertical distribution of porosity (a) and permeability (b) of different depositional facies sandstones.

4.2. Pore Type and Physical Properties

4.2.1. Pore Types of Reservoirs. The main pore type in sandstone reservoir is the residual intergranular pores (maximum facial porosity of 20%, 4.5% on average), and partly secondary pore (maximum facial porosity of 4.5%, 1.5% on average). The residual intergranular pores are cemented by Fe-calcite and filled with kaolinite and calcite (Figures 8(b), 8(c), 8(d), 8(e), and 8(g)). The secondary pores are primarily the intragranular dissolved pore of the feldspar and lithic fragment (Figures 8(e), 8(g), 8(h), and 8(i)), moldic pore, and a little carbonate cement dissolved pores and kaolinite intercrystallite pores. There are a little of intragranular fractures that can be seen in casting thin sections (Figure 8(a)). The pore type of the subaqueous distributary and mouth bar is dominated by the residual intergranular pores, with the intragranular dissolved pores followed (Figure 4(c)). The sheet sand and subaqueous fan sandstone developed more feldspar dissolved pore (Figure 5(c)). The original intergranular pores and dissolved pores are less developed in beach-bar deposits (Figure 5(c)).

4.2.2. Reservoir Physical Property Characteristics and Classification. The measured core porosity ranges from 2.76% to 19.8%, with an average of 12.4%, and the air permeability is from <0.1 mD to 271.45 mD, with an average of 45.8 mD. Porosity and permeability decreased significantly with increasing depth (Figure 9).

According to the porosity and permeability classification standard [56, 57], the reservoirs of different depositional facies are mainly divided into four types: medium porosity and low permeability (type I reservoir), low porosity and

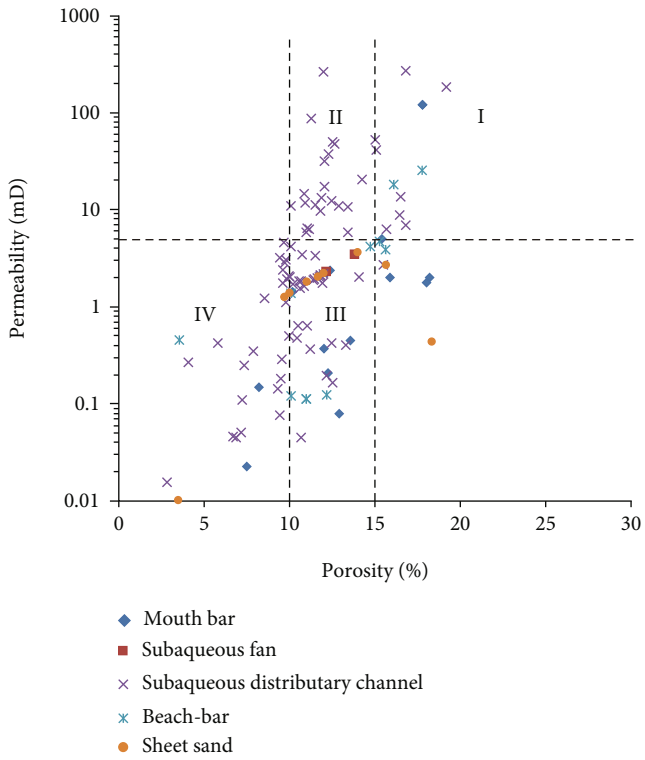

Figure 10: The plot of porosity versus permeability for different depositional facies. I: medium porosity and low permeability; II: low porosity and low permeability; III: low porosity and ultra-low permeability; IV: ultra-low porosity and ultra-low permeability.

low permeability (type II reservoir), low porosity and ultra-low permeability (type III reservoir), and ultra-low porosity and ultra-low permeability (type IV reservoir). Different sedimentary microfacies reservoirs in E_2w can be divided into different reservoir types based on the classification criteria. Subaqueous distributary channel has widely distributed porosity and permeability, and all four reservoir types are developed. The mouth bar and beach-bar sandbodies mainly developed type I and III reservoirs with medium-low porosity and ultra-low permeability, while the physical properties of sheet sand and subaqueous fan are relatively poor, and mainly developed type III reservoir with low porosity and ultra-low permeability. In general, the physical properties of the subaqueous distributary channel, mouth bar, and beach-bar are superior to other facies (Figure 10).

4.3. Diagenesis and Authigenic Mineral Formation

4.3.1. Compaction. Predominant grain contacts in E_2w are point-line (Figures 8(b) and 8(c)) and concave-convex (Figures 8(d) and 8(f)). Such grain contact indicates that the reservoir has undergone intense mechanical compaction and the primary pores have been destroyed.

4.3.2. Cementation. Cementation, the diagenetic process that dissolved minerals precipitate and fill the pore space between sediment particles, can form different authigenic minerals like quartz, carbonate, and clays.

(1) Siliceous Cementation. Secondary quartz, as a kind of common diagenetic mineral, is widely developed in the study area, with a content of 0-6%, and an average of 0.6% (Table 1). Secondary quartz is mainly characterized by quartz overgrowth. Quartz grows beyond the contact point of the detrital particles, and the "dust" line can be seen between the quartz overgrowth and the quartz particle (Figure 8(b)). The quartz overgrowth was encased by kaolinite and early calcite, indicating that it was cemented earlier than the kaolinite and early calcite (Figure 8(b)). The scanning electron micrograph shows that the authigenic quartz coexisted with the illite/smectite mixed layer and illite and blocked the residual intergranular pores (Figures 11(a) and 11(b)).

(2) Carbonate Cementation. The main carbonate cement types in the study area are calcite and Fe-calcite, with a small amount of siderite, dolomite, and Fe-dolomite (Figures 8(b) and 8(e)). The content of carbonate cement varied greatly from 0 to 22%, with an average content of 1.7% (Table 1). The early calcite cement is often extensively developed at the mud-sand interface at the bottom of the distributary channel, with a content of more than 10% (Figure 4 and Table 1). It usually developed at particle contact points, filled the primary pores, and appears red on the stained thin section (Figures 8(b) and 8(c)). The content of Fe-calcite is low, generally <3% (Table 1), and appears dark purple under the stained thin section (Figures 8(d)–8(f)). It usually developed in residual primary intergranular pores and dissolved pores of feldspar, which indicates that the Fe-calcite precipitated later than the dissolution (Figure 8(e)).

(3) Clay Mineral Cementation. Clay minerals widely existed in sandstone reservoirs. According to 37 core samples of E_2w, the content of clay mineral ranges from 2% to 13%, with an average of 4.1% (Table 1). Clay mineral cements are mainly composed of chlorite, kaolinite, illite, and illite/smectite mixed layer. Among them, the illite and chlorite are higher in content (Figure 12).

The chlorite cement content is relatively high, varying from 3% to 32%, and with an average of 14% (Table 2). SEM observations reveal that the main forms of chlorite cemented between sandstone particles are pore filling and sheet, and the crystallization is relatively poor (Figure 8(d)). When the depth exceeds 3200 m, the chlorite content increases significantly, indicating that the smectite may undergo chloritization (Figure 12(a); [58]).

Kaolinite is well crystallized and self-shaped, presenting scattered pseudohexagonal crystals or page-like, vermiform aggregates (Figures 11(c) and 11(d)). Kaolinites fill the intergranular pores or intragranular dissolved pores of feldspar near the feldspar dissolution residue, which indicates that the formation of kaolinites may be related to the feldspar dissolution (Figure 11(c)). The kaolinite content increases significantly within a certain depth range (Figure 12(b)). For example, the kaolinite content in the depth range of 3100-3600 m in well W2 and 3600-3900 m in well W4 is higher, but when the depth exceeds 3900 m, the kaolinite

Table 1: Absolute content of cements.

Cementation type	Siliceous cement	Carbonate cement			Clay mineral cementation
	Secondary quartz	Early calcite cement	Fe-calcite	Total	
Range (%)	0~6	10~22	0~3	0~22	2~13
Average (%)	0.6	13	0.3	1.7	4.1

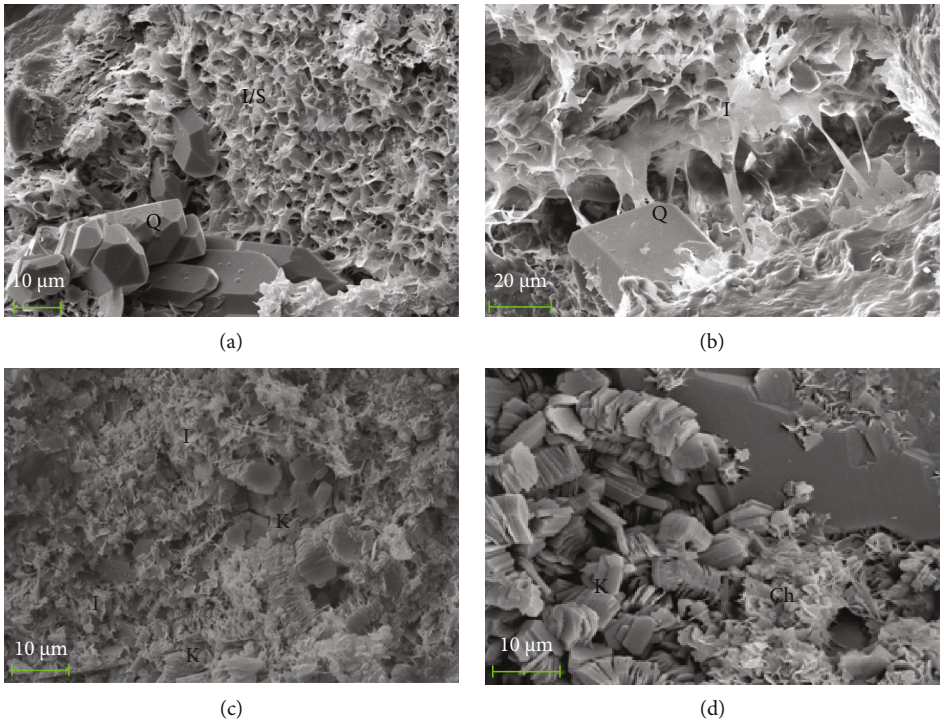

Figure 11: SEM images of the clay minerals of E_2w in the Southern Lufeng depression. (a) The illite/smectite mixed clay minerals with a honeycomb shape attached to the surface of particles, 4155.25 m, W4. (b) The illite takes on the silk-tread form, bridging the pore, 4167.74 m, W4. (c) Silk-tread illite and kaolinite symbiotically block fill intergranular pores, showing that the illite is transformed from the kaolinite, 3092.3 m, W9. (d) Book-like kaolinite fills the intergranular pores, 3897 m, W2. I/S: illite/smectite; Q: quartz; I: illite; K: kaolinite; Ch: chlorite.

content decreases rapidly because the kaolinite is transformed to illite at this depth (Figures 12(b) and 12(c)). The kaolinite content in subaqueous fan, beach-bar, and mouth bar is higher than that in subaqueous distributary channel and sheet sand (Figure 13(a)).

The illite content of E_2w is high and can reach 96% (Table 2). SEM observations reveal illites have two genetic types: one is transformed from smectite, showing honeycomb, messy sheet, and filaments attached to the surface of particles, and the other is transformed from kaolinite, retaining kaolinite's crystal form (Figure 11(c)). The content of the illite/smectite mixed layer is relatively low and the content increases first and then decreases with the increasing of burial depth. When the depth exceeds 3900 m, the content decreases rapidly (Figure 12(d)). This clay mineral is characterized by sheet-like monomer and honeycomb, and cotton aggregate covers the surface of particles (Figure 11(a)).

4.3.3. Metasomatism. Metasomatism is also common in the study area, such as the transformation between clay minerals and feldspar alteration. Smectite may be converted to chlorite and illite with the increase in burial depth (Figures 8 and 12(b)–12(d)). Kaolinite is mainly formed by feldspar alteration distributed near feldspar dissolution residue (Figure 8(g)), and the content reaches the maximum within 3600-3900 m. When the depth exceeds 3900 m, kaolinite changes into illite, and the kaolinite content decreases rapidly, while the illite content increases (Figures 12(b) and 12(c)).

4.3.4. Dissolution. Petrological studies show that dissolved pores are developed in various minerals, such as feldspar, lithic fragment, kaolinite, and calcite, especially feldspar dissolution is obvious (Figures 8(g) and 8(h)).

4.4. Diagenetic Stages and Sequences. Based on the analysis of cast thin sections, scanning electron microscopes, X-ray diffraction, vitrinite reflectance, and other data of the reservoir, it is concluded that the Wenchang Formation is in the middle diagenetic A2 stage [59]. In the early diagenetic A stage, the compaction prevailed, and calcite cementation and silicate cementation occurred in the later stage. In the early diagenetic B stage, compaction and early calcite

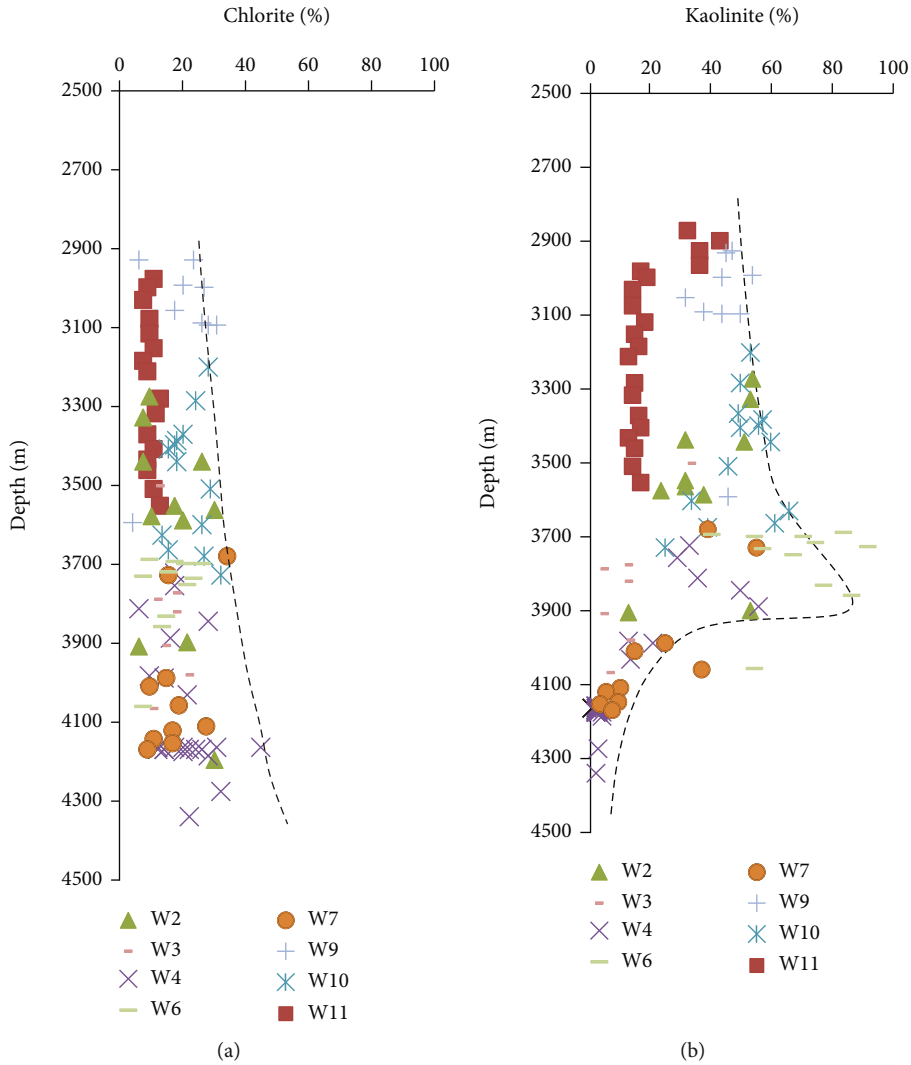

Figure 12: Continued.

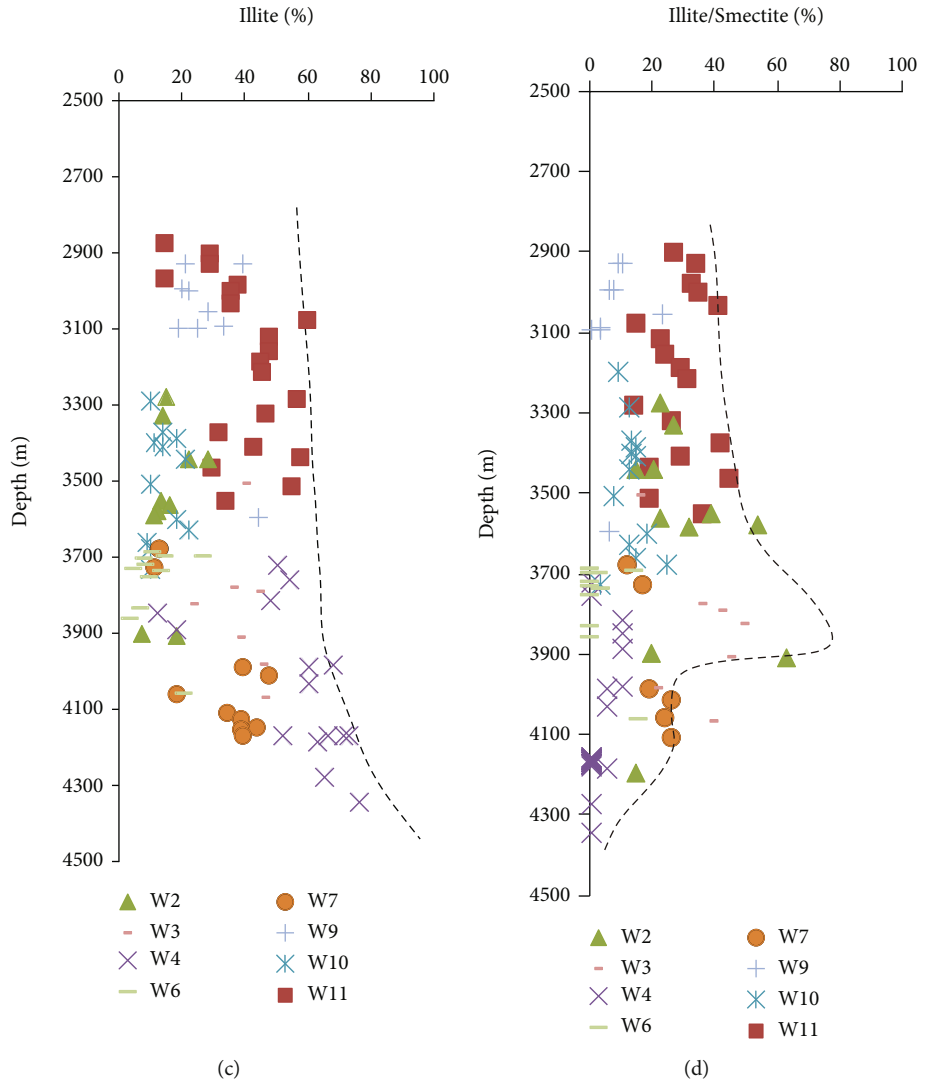

Figure 12: Variation of clay mineral content with depth obtained from XRD experiment.

Table 2: The relative content of clay mineral cement.

Mineral type	Chlorite	Kaolinite	Illite	Illite/smectite
Range (%)	3-32	<30	<96	<18
Average (%)	14	10	65	5

cementation continued, and clay minerals (illite and illite/smectite mixed layer) cementation was widely developed. In the middle diagenetic A1 stage, the compaction was weakened, the silicate cementation was strengthened, and the kaolinite began to precipitate. The organic acid generated by the hydrocarbon generation of the source rock led to the dissolution of feldspar and calcite. In the middle diagenetic A2 stage, the source rock entered the mature stage, and a large amount of oil and gas filled the reservoir pores, weakening the compaction. The cementation of silicate minerals continued to strengthen, and the cementation of chlorite and iron calcite also began to appear. With the gradual weakening of the dissolution of feldspar and calcite, kaolinite began to transform into illite, and the illite content increased rapidly as the kaolinite content decreased.

4.5. The Characteristics of the Anomalously High Porosity. The porosity, greater than the maximum porosity of the normal sandstones for a given lithofacies, age, burial history, and thermal history, is defined as anomalously high porosity [44, 60]. According to the relationship between porosity and the reservoir depth, using the maximum porosity of the reservoir in the vertical direction, it is found that the 3950~4500 m of W4, 4000~4200 m of the W7, and the 3600~3700 m of the W10 developed the anomalously high porosity (Figure 14).

5. Discussion

5.1. Influence of Sedimentation on Reservoir Quality under the Constrain of Sequence Framework. Different sandstone types in different system tracts of the sequence result in different mineral composition and texture, which in turn

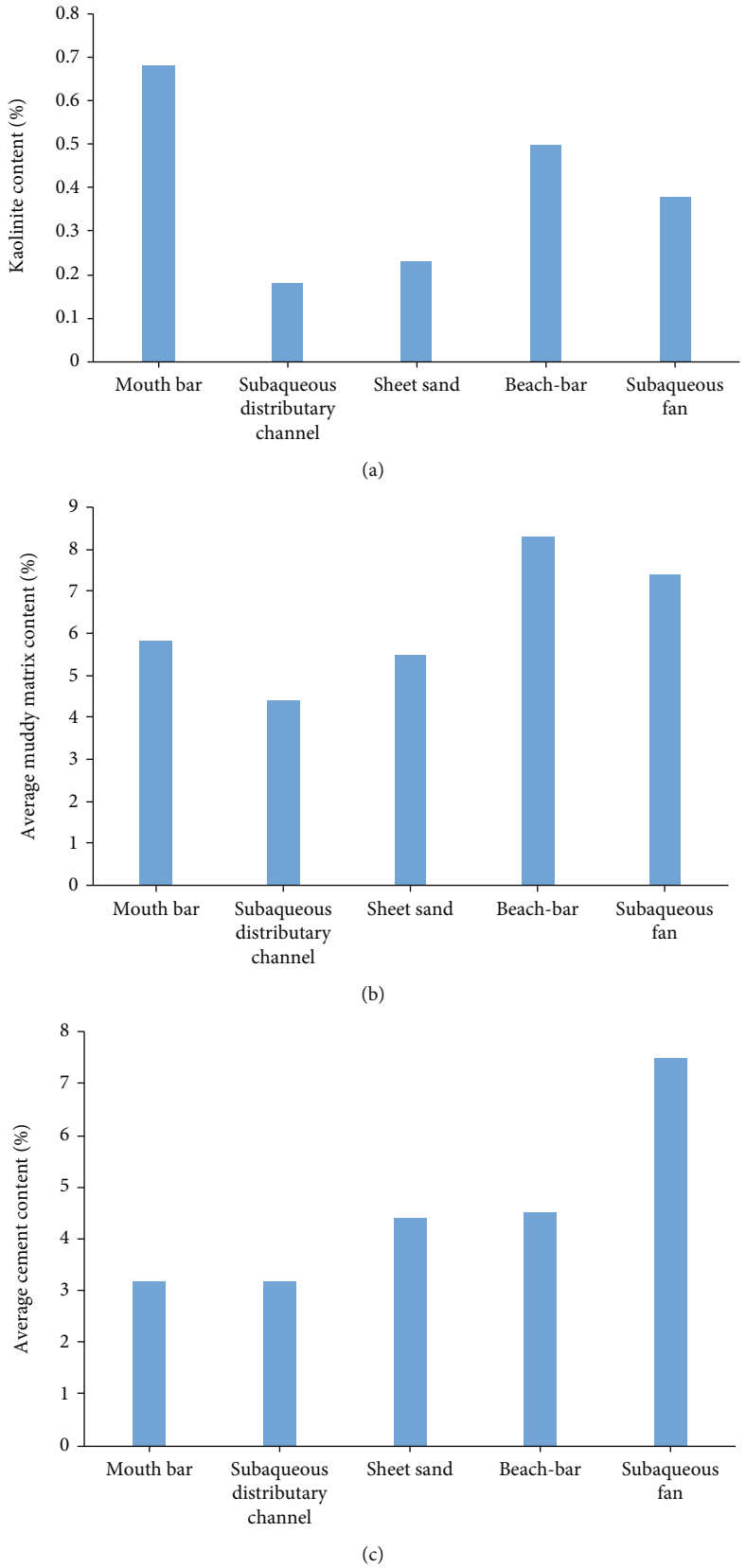

Figure 13: Continued.

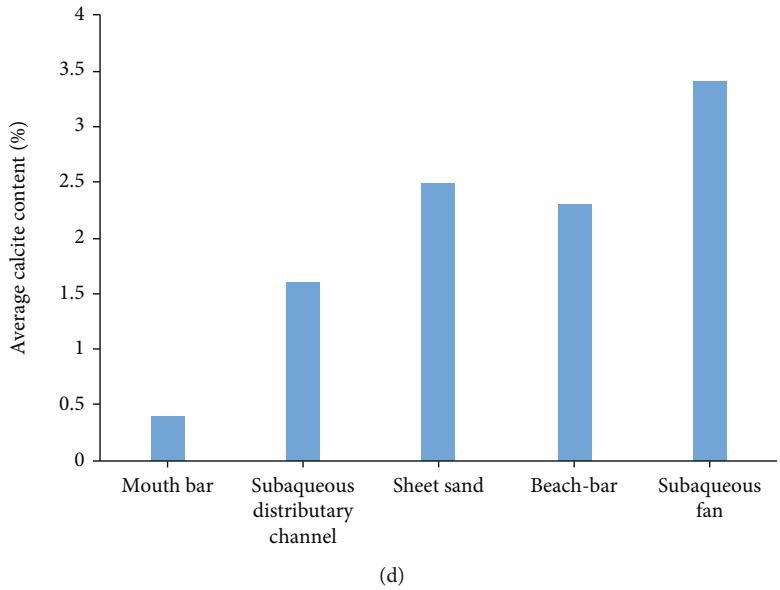

(d)

Figure 13: Histograms show the kaolinite (a), average muddy matrix cement (b), average cement content (c), and average calcite content (d) in the sandstones of different depositional facies.

affects the reservoir diagenetic evolution and reservoir quality differences [11, 13, 61, 62].

The lowstand systems tract (LST) and highstand systems tract (HST) mainly developed braided-delta front sandbodies. The subaqueous distributary channel sandbodies developed in the braided-delta front have different diagenetic evolutions at different positions inside the sandbodies resulting in different reservoir qualities. The sandstone in the bottom part of the subaqueous distributary channel, depositing during a strong hydrodynamic environment, is characterized by coarse grain size, low matrix content, strong anticompaction and dissolution, and favorable reservoir physical characteristics, especially the significant permeability (Figures 4, 10, and 13(b)). The sandstone in the upper part of the subaqueous distributary channel, forming during a relatively weak hydrodynamic environment, is dominated by the characteristics of fine grain size, more muddy matrix, soft lithic fragment, and strong compaction. In this kind of sandstone, primary intergranular pores are difficult to preserve, and the dissolution is weak because the acid fluid cannot enter intergranular pores easily (Figure 4), inducing the reservoir physical characteristics of this kind of sandstone is poor. The mouth bar and sheet sand developed in the delta front are mainly medium-fine sandstones with weak cementation and well-developed primary pores (Figures 4 and 13(c)). This type of sandstone is adjacent to the source rock in spatial distribution; thus, it is easy to be dissolved by the organic acid discharged from the source rock (Figure 4), resulting in relatively high porosity. However, this type of sandstone has a fine particle size, and the permeability is not very high. The TST mainly develops lacustrine beach-bar and subaqueous fan sandstones. These sandstones are characterized by fine particle size, high content of calcite cement, and a high muddy matrix (Figures 5 and 13(b)–13(d)). The reservoir's physical properties are generally poor because of the strong compaction and cementation under the rapid burial conditions.

5.2. The Impact of Diagenesis on Reservoir Development. The diagenesis can change sandstone compositions and reservoir physical properties through compaction, cementation, and dissolution [29, 63–65].

5.2.1. Influence of Compaction on Reservoir Qualities of Different Microfacies Sandbodies. The effect of compaction on the reservoir space of sandbodies in different sedimentary microfacies is different [59, 66]. The impact of compaction on the reservoir qualities of subaqueous distributary channel and mouth bar is weaker than that of beach-bar and subaqueous fan sandstone (Figure 15). This is mainly because the detrital components of beach-bar and subaqueous fan sandbodies are more complex and the contents of argillaceous matrix and soft lithic fragment are relatively large, resulting in weak anti-compaction (Figure 4). Under compaction, the porosity decreases rapidly and the physical properties are poor. For subaqueous fan and beach-bar sandbodies, the cementation is stronger, which can also inhibit the pore reduction induced by compaction to a certain extent (Figure 5).

5.2.2. Influence of Different Types of Cementation on Reservoir Space. Cementation plays a destructive role in reservoir development. E_2w mainly developed the early calcite cementation, quartz overgrowth, late Fe-calcite cementation, Fe-dolomite cementation, and clay mineral cementation (Figures 8(c)–8(e)). The early calcite mainly occurred at the bottom of the subaqueous distributary channel close to sand-shale interface and beach-bar sandstone (Figure 4(c)), which led to poor physical properties of this part of the sandstone. In other samples, the facial porosity loss by the

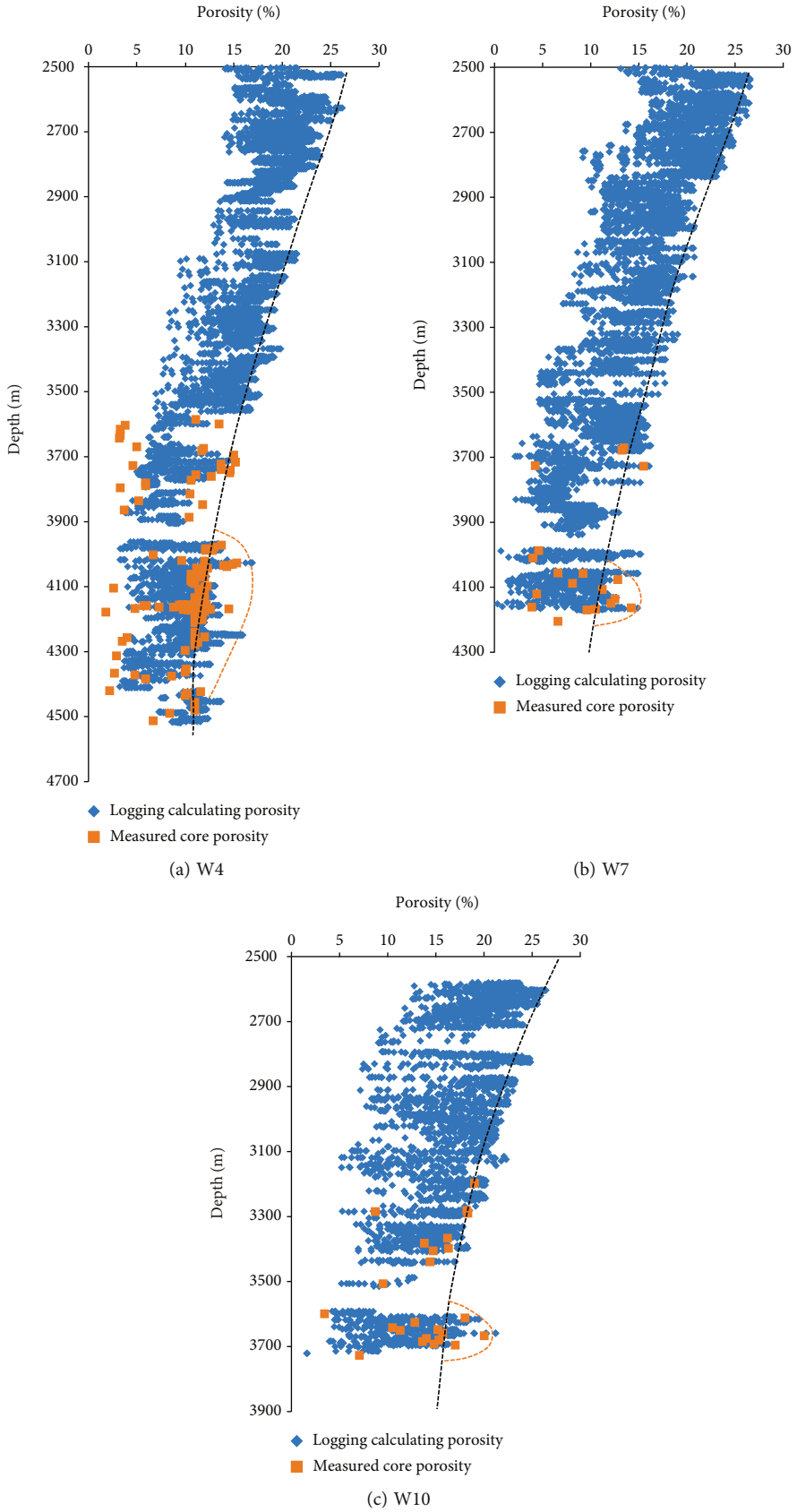

Figure 14: The relationship between the depth and the porosity (the logging calculating porosity and the measured core porosity).

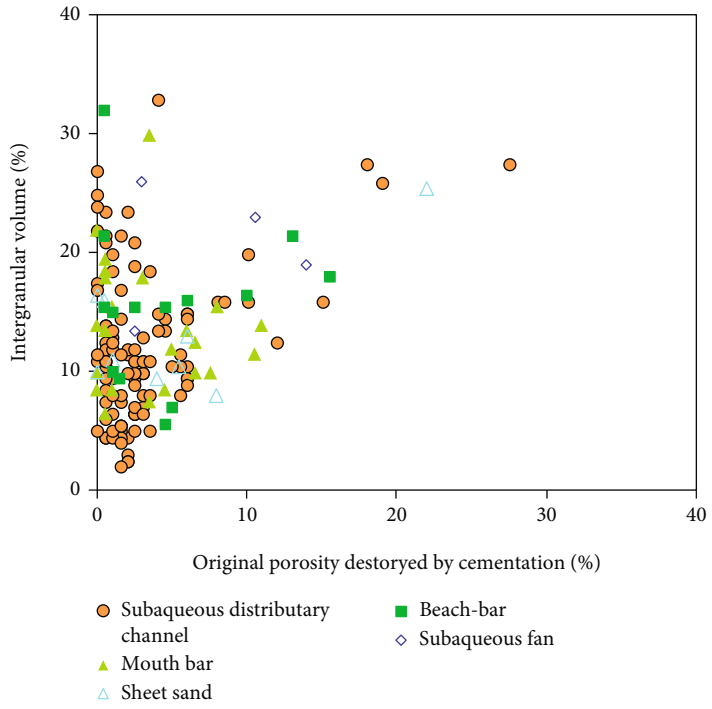

Figure 15: The plot of intergranular volume vs volume content of cements shows the relative importance of compaction and cementation in the porosity reduction of E_2w sandstones.

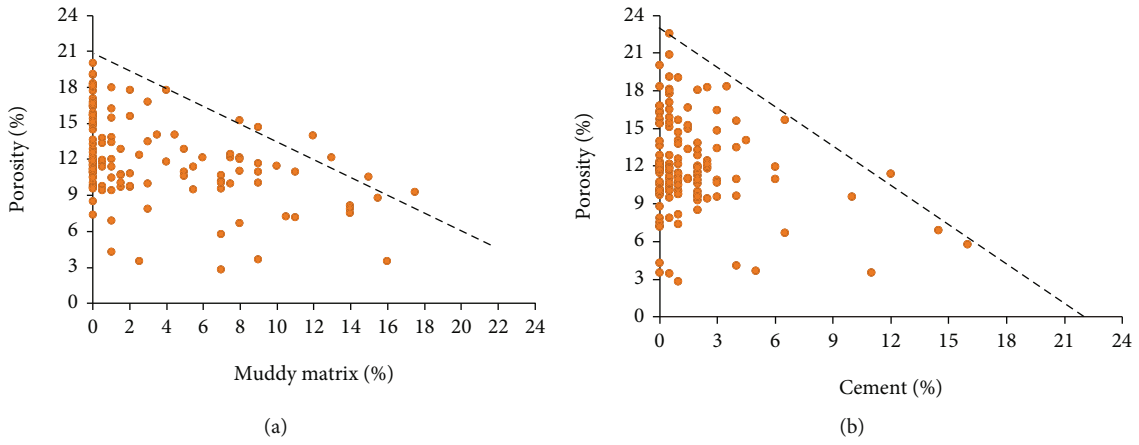

Figure 16: Influence of muddy matrix and cement on the measured porosity. (a) The porosity versus the muddy matrix content. (b) The porosity versus the cement content.

early calcite is less than 3% (Figure 13(d)). The quartz overgrowth is also an important reason for the porosity loss [67, 68]. However, the quartz overgrowth in E_2w is not significant, with an average content of less than 1%. Clay minerals are more likely to block the pore throat and reduce the pore connectivity, resulting in poor reservoir permeability [69, 70]. For example, illite and illite/smectite mixed layer infill the intergranular pores or wrapped the particles (Figures 11(a) and 11(b)), resulting in reduced porosity and pore connectivity. As the clay mineral content and cement content increase, the porosity decreases obviously (Figures 16(a) and 16(b)). In general, the authigenic minerals in the sandstone reservoir of E_2w are limited, and the cement content of most sandstone samples is less than 4% (Figure 14(c)). Therefore, the influence of authigenic minerals on the reservoir's physical properties is relatively weak.

5.2.3. Influence of Dissolution on Reservoir Space. Dissolution acts as a constructive role in the process of reservoir development. The petrological study shows that feldspar, calcite, rock debris, and kaolinite all undergo certain dissolution, especially feldspar (Figures 8(g) and 8(h)). Therefore, the dissolution mechanism of aluminosilicate minerals and calcite has been discussed in detail in this study, which usually includes two kinds of dissolution: atmospheric fresh

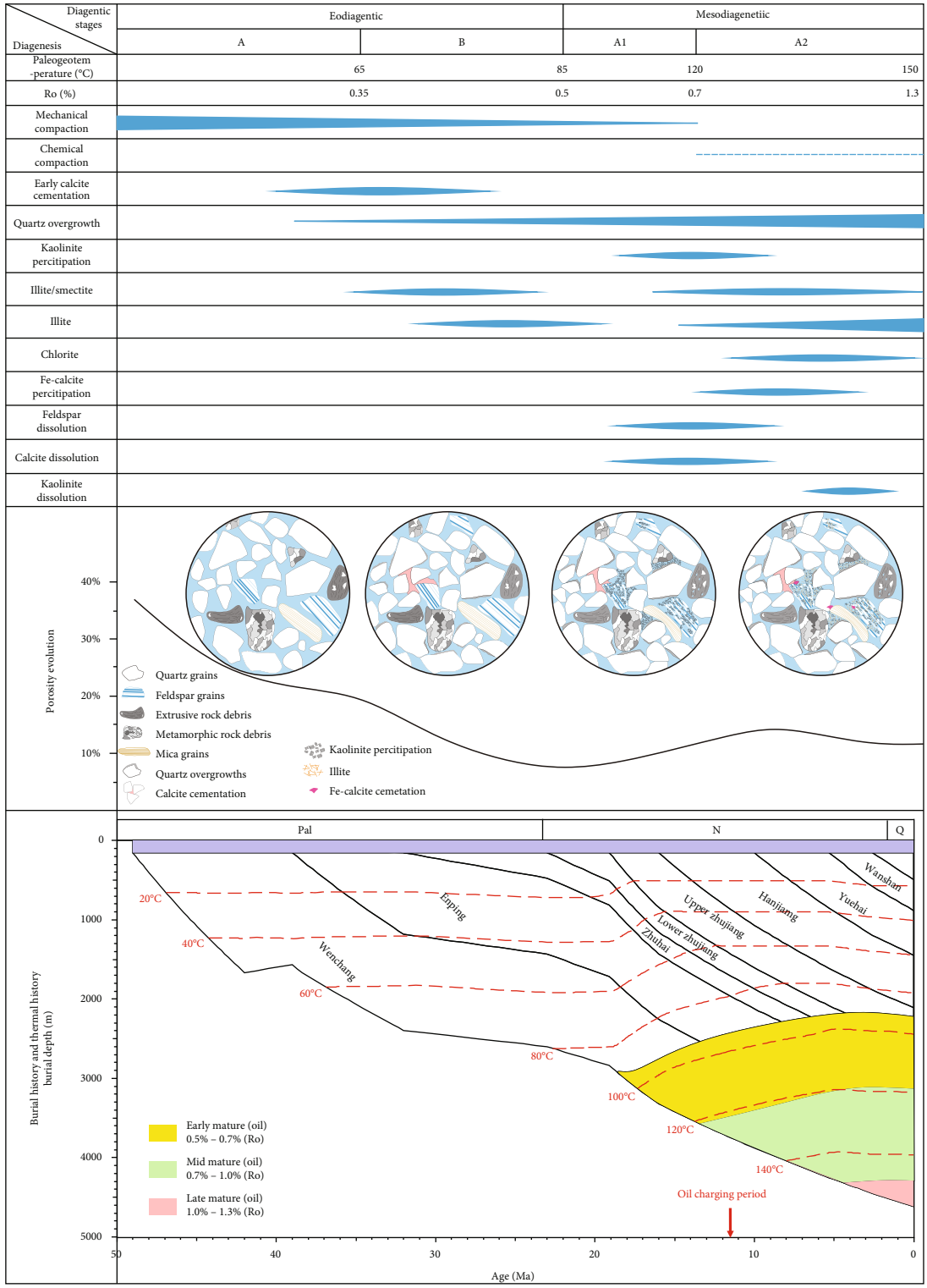

Figure 17: Diagenetic evolution, burial history, and thermal history of E_2w sandstones in the Lufeng southern depression.

water and organic acids [8, 33, 71, 72]. Atmospheric water dissolution usually occurred at the shallow burial stage. It mainly dissolved the calcite cement formed in the early stage, and the secondary pores often have poor pore structure characteristics under the influence of late diagenesis. With the burial depth of E_2w increased to 2900 m, the reservoir temperature could reach 80°C (Figure 17). At this time, the source rock began to mature, and the thermal degradation of the organic matter caused the kerogen to form and discharge organic acid outward (Figure 17). The organic acid entered sandstones causing the dissolution of aluminosilicate minerals and calcite cement, especially the feldspar

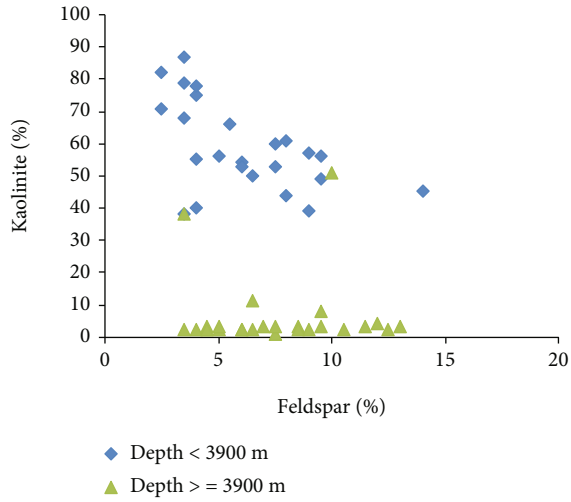

Figure 18: The plot of kaolinite content versus feldspar content for the sandstones of E_2w.

altered into kaolinite [71]. When the burial depth is less than 3900 m, there is a significant negative correlation between the kaolinite content and the feldspar content (Figure 18), indicating the dissolution that occurred in sandstones of E_2w is related to the organic acid. The vertical distribution of facial porosity and secondary facial porosity shows that the proportion of secondary facial porosity to total facial porosity increases gradually with the depth (Figure 19). Although the facial porosity of secondary dissolved pores of E_2w is only 0.5%-4.5%, they account for 4%-53% of the total facial porosity. The proportion of secondary porosity is higher and can even reach 30%~50% when the burial depth is more than 4000 m (Figure 19). All of these evidences indicate that the secondary dissolved pores have an important improvement on E_2w reservoir porosity.

5.3. The Genesis of the Anomalously High Porosity and High-Quality Reservoirs. The chlorite clay coats, microcrystalline coats, hydrocarbon charging, fluid overpressure, and dissolution can all cause anomalously high porosity in the middle and deep reservoirs [17, 33, 60, 73]. The anomalously high porosity in our research area is primarily found in the subaqueous distributary channel and mouth bar in the LST of SSQ2, corresponding to Ew_5.

5.3.1. The LST Distributary Channel and Mouth Bar Sandbodies Are the Dominant Facies for the Anomalously High Porosity and High-Quality Reservoirs. The anomalously high porosity is usually developed in subaqueous distributary channel and mouth bar sandstones that are deposited in strong hydrodynamic conditions. These sandstones contain high quartz content, usually higher than 80%, so that they can retain a higher content of intergranular pore space even after compaction; thus, high quartz content is the basis for the ultimate pervasive intergranular pores [74]. Due to the high hydrodynamic sedimentary conditions, these sandstones are coarse grain in size (primarily pebbly coarse sandstone, coarse-medium sandstone), good sorting, low content of muddy matrix, high primary porosity and permeability, and strong anti-compaction capability. At the late diagenetic stage, acidic fluid is also prone to enter this kind of reservoir for dissolution. Therefore, the subaqueous distributary channel and mouth bar in LST are very favorable for the formation of high-quality reservoirs.

5.3.2. Secondary Pores Caused by Hydrocarbon Charging Are the Cause of Abnormally High Porosity and High-Quality Reservoirs. The pores for the anomalously high porosity are composed of not only a large number of primary intergranular pores but also many secondary dissolved pores. According to the facial porosity statistics from the thin sections, the facial porosity of the secondary dissolved pores account for 30% of the anomalously high porosity (Figure 19), which is higher than that in normal sandstones, indicating that the secondary dissolved pores are an important reason for the development of anomalously high porosity.

The Ew_4 in the southern Lufeng depression is the main source rock member. With the burial depth of source rock increased to 2700 m, vitrinite reflectance (Ro) reached about 0.5%, the source rock began to enter the hydrocarbon generation threshold, and the organic matter began to release a large number of organic acids (Figure 17). With the further increase of burial depth, the maturity of source rock also increased accordingly. When the burial depth reached 3300 m, the source rock reached the oil generation peak (Figure 17). Along with oil and gas, a large number of organic acids preferentially entered the sandstone reservoir with good porosity and permeability in LST, resulting in the dissolution of feldspar and lithic fragments and resistance to compaction to a certain extent. With the dissolution of feldspar, the content decreased, and the secondary dissolved pores and kaolinite increased correspondingly (Figures 17–19). The depth range of the anomalously high porosity just matches the source rock depth during peak oil generation (Figure 17), which is the favorable factor for the development of secondary pores.

5.3.3. Hydrocarbon Charging Prevents Abnormally High Porosity and High-Quality Reservoirs from Being Damaged by Late Diagenesis. Hydrocarbon charging inhibits the late diagenesis and protects the primary intergranular pores, which is conducive to the formation of the anomalously high porosity reservoirs [44, 75]. The anomalously high porosity reservoir in our research area is mainly developed in the oil-bearing strata Ew_5 near source rock Ew_4, indicating that the development of anomalously high porosity may be related to the hydrocarbon charging. According to the hydrocarbon generation and charging history of E_2w in the Lufeng depression, hydrocarbon generated by source rock Ew_4 at the peak hydrocarbon generation period migrated vertically and laterally along the widely developed sandbodies of LST and faults and accumulated in sand bodies of Ew_5 at the time of 13 Ma (Figure 17; [76]). This indicated that the oil-bearing sandstone had been charged and accumulated oil before entering deep burial (Figure 14), which inhibited the physical and chemical compaction and cementation in deep burial stage, and protected primary intergranular pores and secondary dissolved pores. In addition, the

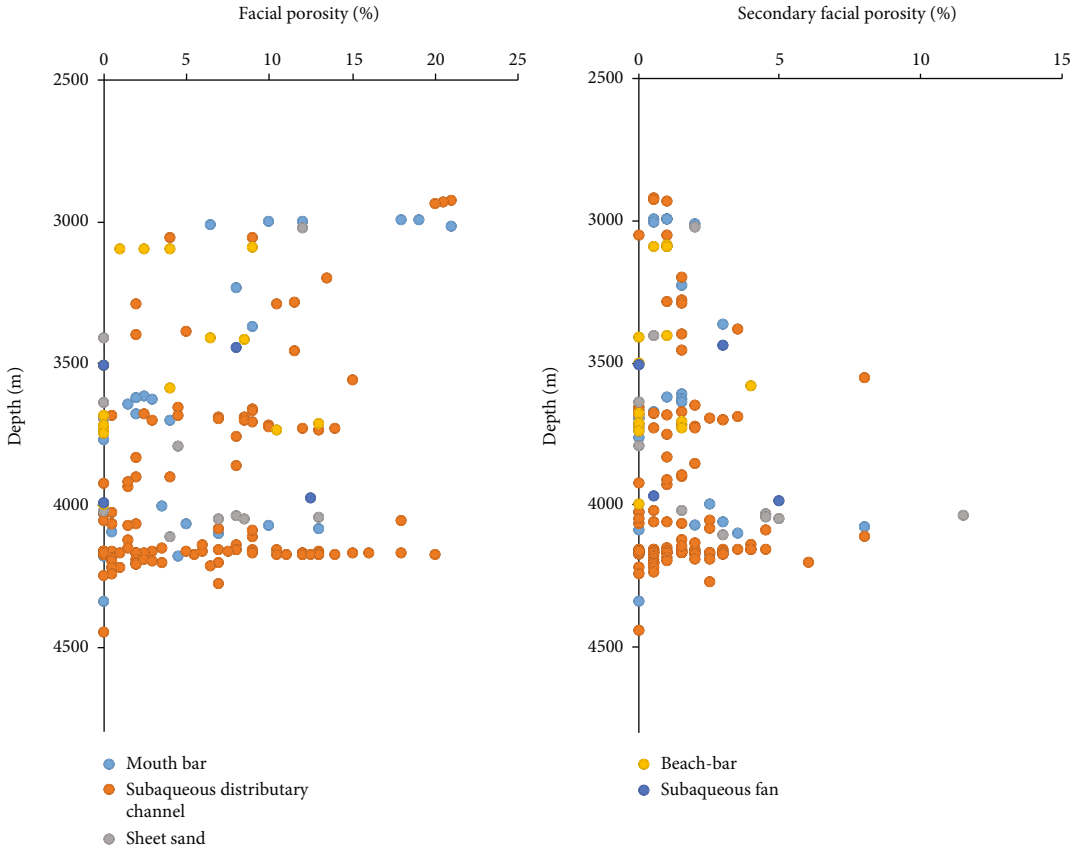

Figure 19: The vertical distribution of facial porosity and secondary facial porosity with different depositional facies.

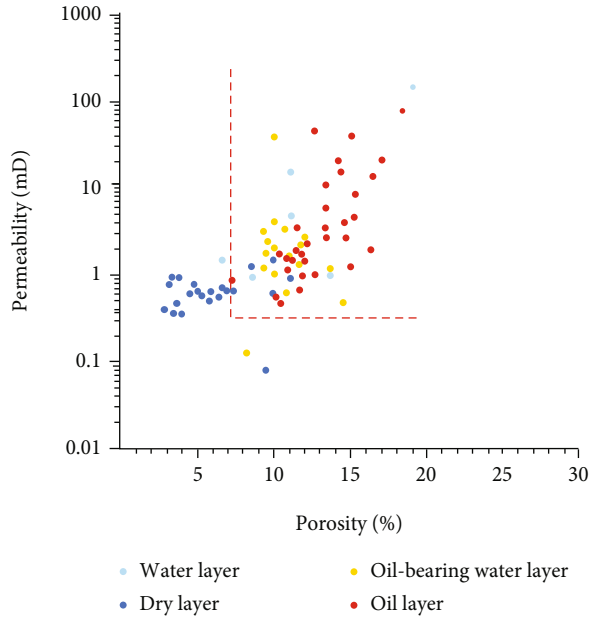

Figure 20: The plot of porosity versus permeability for sandstones with different oiliness.

dissolution of uncompacted feldspar residues by organic acid also indicated that the Ew_5 sandstones had not undergone intense compaction during the late diagenetic stage (Figures 8(g) and 8(h)). The relatively high content of intergranular pores, low cement content, and high porosity and permeability of oil-bearing sandstones indicate that hydrocarbon charging inhibits the late diagenesis and protects the reservoir space. (Figures 4, 13(c), and 20).

6. Conclusion

(1) The lithology of E_2w sandstone reservoir is mainly lithic quartz sandstone, and the pore types are dominated by residual intergranular pores and intragranular dissolved pores. The average porosity of the reservoir is 12.4% and the average permeability is 45.8 mD. The sandstone reservoirs of E_2w have undergone a series of diagenetic processes and are currently in the middle diagenetic A2 stage. According to the difference of physical properties, the E_2w reservoir can be divided into four types, of which high-quality and abnormally high porosity reservoirs are mainly developed in LST of SSQ2, corresponding to Ew_5

(2) Different microfacies sandstone reservoirs in different system tracts have different material compositions and later diagenetic evolution. The subaqueous distributary channel and mouth bar sandstones deposited in LST and HST display coarse grain size, good sorting, high quartz content, and low muddy matrix content, which induced strong anti-compaction capability and a higher content of intergranular pore space.

Affected by different diagenetic evolutions, the reservoir quality in the bottom part of subaqueous distributary channel is better than that in the upper part. The subaqueous distributary channel and mouth bar sandstones in LST of SSQ2 are adjacent to Ew_4 source rock in TST of SSQ2, which makes it easier for organic acids generated during the peak period of hydrocarbon generation and expulsion to enter these sandstone reservoirs for dissolution, resulting in the formation of anomalously high porosity and high-quality reservoirs. The beach-bar and subaqueous fan sandstones developed in TST have fine particle size and high muddy matrix content, which result in strong compaction and cementation, and weak dissolution, and finally poor reservoir physical properties

(3) Compaction and cementation have different destructive effects on the pores of different sedimentary microfacies reservoirs. The compaction strength of subaqueous distributary channel and mouth bar sandstones is weaker than that of beach-bar and subaqueous fan sandstones due to their high quartz content and hydrocarbon charging. Quartz overgrowth, calcite cementation, and clay mineral cementation are widely developed in the area, but due to its low content, it has a relatively weak effect on the reservoir's physical properties. Dissolution, especially organic acid dissolution of feldspar and calcite cementation, leads to the formation of a large number of secondary dissolved pores. Organic acid dissolution, accompanied by hydrocarbon charging before deep burial, led to the formation of abnormally high porosity and high-quality reservoirs in LST of SSQ2

Data Availability

The data in this study are confidential and cannot be disclosed.

Conflicts of Interest

The authors declare that they have no conflicts of interest.

Acknowledgments

The authors are grateful to the staffs from Shenzhen Branch, CNOOC, for their kindly assistance in the collection of core samples and other data. This research work is supported by the National Natural Science Foundation of China (No. 41902125) and the Shenzhen Branch of CNOOC.

References

[1] G. Guo, Y. H. Deng, J. F. Wu et al., "Evaluation of latent Paleogene hydrocarbon-rich sags in the northern sag belt, Zhu I depression, Pearl River Mouth basin," *China Offshore Oil and Gas*, vol. 26, no. 1, pp. 17–23, 2014.

[2] B. Z. Xian, Z. Y. Lu, and Y. Q. She, "Sedimentary and reservoir characteristics of glutenite in Yan 18-Yong 921area, steep slope of Dongying Sag," *Lithologic Reservoirs*, vol. 26, no. 4, pp. 28–35, 2014.

[3] X. Zhu, J. Ge, C. Wu et al., "Reservoir characteristics and main controlling factors of deep sandstone in Lufeng sag, Pearl River Mouth Basin," *Acta Petrolei Sinica*, vol. 40, no. S1, pp. 70–80, 2019.

[4] D. Z. Ren, L. T. Ma, D. K. Liu, J. Tao, X. Q. Liu, and R. J. Zhang, "Control mechanism and parameter simulation of oil-water properties on spontaneous imbibition efficiency of tight sandstone reservoir," *Frontiers of Physics*, vol. 10, no. 10, article 829763, 2022.

[5] P. K. Sun, H. M. Xu, H. Q. Zhu et al., "Investigation of pore-type heterogeneity and its control on microscopic remaining oil distribution in deeply buried marine clastic reservoirs," *Marine and Petroleum Geology*, vol. 123, article 104750, 2021.

[6] M. Virolle, H. Féniès, B. Brigaud et al., "Facies associations, detrital clay grain coats and mineralogical characterization of the Gironde estuary tidal bars: a modern analogue for deeply buried estuarine sandstone reservoirs," *Marine and Petroleum Geology*, vol. 114, pp. 104225–104225, 2020.

[7] G. Bi, C. Lyu, C. Li et al., "Impact of early hydrocarbon charge on the diagenetic history and reservoir quality of the Central Canyon sandstones in the Qiongdongnan Basin, South China Sea," *Journal of Asian Earth Sciences*, vol. 185, article 104022, 2019.

[8] K. Bjørlykke and J. Jahren, "Open or closed geochemical systems during diagenesis in sedimentary basins: constraints on mass transfer during diagenesis and the prediction of porosity in sandstone and carbonate reservoirs," *AAPG Bulletin*, vol. 96, no. 12, pp. 2193–2214, 2012.

[9] K. Bjørlykke, "Relationships between depositional environments, burial history and rock properties. Some principal aspects of diagenetic process in sedimentary basins," *Sedimentary Geology*, vol. 301, pp. 1–14, 2014.

[10] B. V. Dung, H. A. Tuan, N. Van Kieu, H. Q. Man, N. T. Thanh Thuy, and P. T. Dieu Huyen, "Depositional environment and reservoir quality of Miocene sediments in the central part of the Nam Con Son Basin, southern Vietnam shelf," *Marine and Petroleum Geology*, vol. 97, pp. 672–689, 2018.

[11] M. A. K. El-Ghali, S. Morad, H. Mansurbeg et al., "Distribution of diagenetic alterations within depositional facies and sequence stratigraphic framework of fluvial sandstones: evidence from the Petrohan Terrigenous Group, Lower Triassic, NW Bulgaria," *Marine and Petroleum Geology*, vol. 26, no. 7, pp. 1212–1227, 2009.

[12] R. H. Lander and O. Walderhaug, "Predicting porosity through simulating sandstone compaction and quartz cementation," *AAPG Bulletin*, vol. 83, pp. 433–449, 1999.

[13] S. Morad, K. Al-Ramadan, J. M. Ketzer, and L. De Ros, "The impact of diagenesis on the heterogeneity of sandstone reservoirs: a review of the role of depositional facies and sequence stratigraphy," *AAPG Bulletin*, vol. 94, no. 8, pp. 1267–1309, 2010.

[14] S. Morad, J. R. M. Ketzer, and L. F. De Ros, "Spatial and temporal distribution of diagenetic alterations in siliciclastic rocks: implications for mass transfer in sedimentary basins," *Sedimentology*, vol. 47, pp. 95–120, 2000.

[15] J. J. O'brien and I. Lerche, "The preservation of primary porosity through hydrocarbon entrapment during burial," *SPE Formation Evaluation*, vol. 1, no. 3, pp. 295–299, 1986.

[16] M. J. Osborne and R. E. Swarbrick, "Diagenesis in North Sea HPHT clastic reservoirs – consequences for porosity and overpressure prediction," *Marine and Petroleum Geology*, vol. 16, no. 4, pp. 337–353, 1999.

[17] M. Ramm, A. W. Forsberg, and J. S. Jahrens, "Porosity-depth trends in deeply buried Upper Jurassic reservoirs in the Norwegian Central Graben: an example of porosity preservation beneath the normal economic basement by grain-coating microquartz," in *Reservoir Quality Prediction in Sandstones and Carbonates*, J. A. Kupecz, J. Gluyas, and S. Bloch, Eds., vol. 69, pp. 177–199, AAPG Memoir, 1997.

[18] D. Z. Ren, H. P. Zhang, Z. Z. Wang, B. Y. Ge, D. K. Liu, and R. J. Zhang, "Experimental study on microscale simulation of oil accumulation in sandstone reservoir," *Frontiers of Physics*, vol. 10, no. 10, article 841989, 2022.

[19] X. Wang, S. He, S. Jones et al., "Overpressure and its positive effect in deep sandstone reservoir quality of Bozhong Depression, offshore Bohai Bay Basin, China," *Journal of Petroleum Science and Engineering*, vol. 182, pp. 106362–106362, 2019.

[20] D. Beard and P. Weyl, "Influence of texture on porosity and permeability of unconsolidated sand," *AAPG Bulletin*, vol. 57, pp. 349–369, 1973.

[21] E. D. Pittman and R. E. Larese, "Compaction of lithic sands: experimental results and applications (1)," *Bulletin of the American Association of Petroleum Geologists*, vol. 75, no. 8, pp. 1279–1299, 1991.

[22] G. Sheng, Y. Su, and W. Wang, "A new fractal approach for describing induced-fracture porosity/permeability/ compressibility in stimulated unconventional reservoirs," *Journal of Petroleum Science and Engineering*, vol. 179, pp. 855–866, 2019.

[23] G. W. Wang, X. C. Chang, W. Yin, Y. Li, and T. T. Song, "Impact of diagenesis on reservoir quality and heterogeneity of the Upper Triassic Chang 8 tight oil sandstones in the Zhenjing area, Ordos Basin, China," *Marine and Petroleum Geology*, vol. 83, pp. 84–96, 2017.

[24] K. Al-Ramadan, S. Morad, J. N. Proust, and I. S. Al-Aasm, "Distribution of diagenetic alterations in siliciclastic shoreface deposits within a sequence stratigraphic framework: evidence from the Upper Jurassic, Boulonnais, NW France," *Journal of Sedimentary Research*, vol. 75, no. 5, pp. 943–959, 2005.

[25] L. T. Cao, Y. B. Yao, C. Cui, and Q. P. Sun, "Characteristics of in-situ stress and its controls on coalbed methane development in the southeastern Qinshui Basin, North China," *Energy Geoscience*, vol. 1, no. 1-2, pp. 69–80, 2020.

[26] K. G. Taylor, R. L. Gawthorpe, and J. C. Van, "Stratigraphic control on laterally persistent cementation, Book Cliffs, Utah," *Journal of the Geological Society*, vol. 152, no. 2, pp. 225–228, 1995.

[27] J. M. Ajdukiewicz and R. H. Lander, "Sandstone reservoir quality prediction: the state of the art," *AAPG Bulletin*, vol. 94, no. 8, pp. 1083–1091, 2010.

[28] J. Lai, G. W. Wang, Y. Chai, Y. Ran, and X. Zhang, "Depositional and diagenetic controls on pore structure of tight gas sandstone reservoirs: evidence from lower cretaceous Bashijiqike formation in Kelasu thrust belts, Kuqa depression in Tarim basin of West China," *Resource Geology*, vol. 65, no. 2, pp. 55–75, 2015.

[29] A. G. Oluwadebi, K. G. Taylor, and P. J. Dowey, "Diagenetic controls on the reservoir quality of the tight gas Collyhurst Sandstone Formation, Lower Permian, East Irish Sea Basin, United Kingdom," *Sedimentary geology*, vol. 371, pp. 55–74, 2018.

[30] P. K. Sun, H. M. Xu, Q. F. Dou et al., "Investigation of pore-type heterogeneity and its inherent genetic mechanisms in deeply buried carbonate reservoirs based on some analytical methods of rock physics," *Journal of Natural Gas Science and Engineering*, vol. 27, pp. 385–398, 2015.

[31] K. Bjørlykke, M. Ramm, and G. C. Saigal, "Sandstone diagenesis and porosity modification during basin evolution," *Geologische Rundschau*, vol. 78, no. 1, pp. 243–268, 1989.

[32] M. Giles, "Mass transfer and problems of secondary porosity creation in deeply buried hydrocarbon reservoirs," *Marine and Petroleum Geology*, vol. 4, no. 3, pp. 188–204, 1987.

[33] V. Schmidt and D. A. McDonald, "The role of secondary porosity in the course of sandstone diagenesis," *SEPM Special Publication*, vol. 26, pp. 175–207, 1979.

[34] P. K. Sun, H. Q. Zhu, H. M. Xu, X. N. Hu, and L. Tian, "Factors affecting the nanopore structure and methane adsorption capacity of organic-rich marine shales in Zhaotong area, Southern Sichuan Basin," *Interpretation*, vol. 8, no. 2, pp. T403–T419, 2020.

[35] X. Zhang, C. M. Lin, Z. Y. Chen, F. Pan, J. Zhou, and H. Yu, "The reservoir characteristics of Chang 8 oil layer group from the Yanchang Formation in Zhenjing area, Ordos Basin," *Geological Journal of China Universities*, vol. 18, no. 2, pp. 328–340, 2012.

[36] L. B. Jia, D. K. Zhong, Y. L. Ji et al., "Architecture of tectonic sequences, depositional systems, and tectonic controls of the sedimentary fills of the rift-related Wenchang Formation in the Lufeng Depression, Pearl River Mouth Basin, China," *Geological Journal*, vol. 54, no. 4, pp. 1950–1975, 2019.

[37] Y. Jia, C. Lin, K. A. Eriksson, C. Niu, H. Li, and P. Zhang, "Fault control on depositional systems and sequence stratigraphic architecture in a multiphase, rifted, lacustrine basin: a case study from the paleogene of the central Bohai Bay Basin, northeast China," *Marine and Petroleum Geology*, vol. 101, pp. 459–475, 2019.

[38] Y. Zhou, Y. L. Ji, J. D. Pigott, Q. A. Meng, and W. Lu, "Tectono-stratigraphy of Lower Cretaceous Tanan sub-basin, Tamtsag Basin, Mongolia: sequence architecture, depositional systems and controls on sediment infill," *Marine and Petroleum Geology*, vol. 49, pp. 176–202, 2014.

[39] X. N. Xie and L. G. Ge, "Sequence stratigraphic model in nearshore fault basin-case study on the rifting stage of Qiongdongnan Basin," *Scientia Geologica Sinica*, vol. 32, no. 1, pp. 47–55, 1997.

[40] J. M. Ajdukiewicz and R. E. Larese, "How clay grain coats inhibit quartz cement and preserve porosity in deeply buried sandstones: observations and experiments," *AAPG Bulletin*, vol. 96, no. 11, pp. 2091–2119, 2012.

[41] R. Gaupp, A. Matter, J. Platt, K. Ramseyer, and J. Walzebuck, "Diagenesis and fluid evolution of deeply buried Permian (Rotliegende) gas reservoirs, northwest Germany," *AAPG Bulletin*, vol. 77, pp. 1111–1128, 1993.

[42] S. R. O'Neill, S. J. Jones, P. J. Kamp, R. E. Swarbrick, and J. G. Gluyas, "Pore pressure and reservoir quality evolution in the deep Taranaki Basin, New Zealand," *Marine and Petroleum Geology*, vol. 98, pp. 815–835, 2018.

[43] X. W. Zhang, X. Q. Pang, C. J. Li et al., "Geological characteristics, formation conditions and accumulation model of deep and ultra-deep, high-porosity an ad high-permeability clastic

reservoirs: a case study of Gulf of Mexico Basin," *Acta Petrolei Sinica*, vol. 42, no. 4, pp. 466–480, 2021.

[44] J. D. Bloch, R. H. Lander, and L. Bonell, "Anomalously high porosity and permeability in deeply buried sandstone reservoirs: origin and predictability," *AAPG Bulletin*, vol. 86, pp. 301–328, 2002.

[45] J. L. Li, "Diagenesis evolution characteristics of deep buried glutenite reservoir bed in the Dongying sag, the Bohai Bay Basin," *Petroleum Geology & Experiment*, vol. 30, no. 3, pp. 252–255, 2008.

[46] T. R. Taylor, M. R. Giles, L. A. Hathon et al., "Sandstone diagenesis and reservoir quality prediction: models, myths, and reality," *AAPG Bulletin*, vol. 94, no. 8, pp. 1093–1132, 2010.

[47] C. M. Chen, "Petroleum geology and conditions for hydrocarbon accumulation in the eastern pearl river mouth basin," *China Offshore Oil and Gas (Geology)*, vol. 14, no. 2, pp. 73–83, 2000.

[48] D. Wu, H. Li, L. Jiang et al., "Diagenesis and reservoir quality in tight gas bearing sandstones of a tidally influenced fan delta deposit: the Oligocene Zhuhai Formation, western Pearl River Mouth Basin, South China Sea," *Marine and Petroleum Geology*, vol. 107, pp. 278–300, 2019.

[49] B. J. Guo, J. S. Xie, and F. D. Xiang, "The study of the petroleum system in the Zhu 1 Depression in Pearl River Mouth Basin," *China Offshore Oil and Gas*, vol. 1, pp. 2–9, 2000.

[50] H. S. Shi, J. Z. Zhu, Z. L. Jiang, Y. Shu, T. J. Xie, and J. Y. Wu, "Hydrocarbon resources reassessment in Zhu I depression, Pearl River Mouth basin," *China Offshore Oil and Gas*, vol. 21, no. 1, pp. 9–14, 2009.

[51] J. Ge, X. Zhu, X. Zhao, J. Liao, B. Ma, and B. G. Jones, "Tectono-sedimentary signature of the second rift phase in multiphase rifts: a case study in the Lufeng Depression (38-33.9 Ma), Pearl River Mouth Basin, South China Sea," *Marine and Petroleum Geology*, vol. 114, article 104218, 2020.

[52] Y. G. Hou, S. He, J. E. Ni, and B. J. Wang, "Tectono-sequence stratigraphic analysis on Paleogene Shahejie Formation in the Banqiao sub-basin, eastern China," *Marine and Petroleum Geology*, vol. 36, no. 1, pp. 100–117, 2012.

[53] J. A. D. Dickson, "A modified staining technique for carbonates in thin section," *Nature*, vol. 205, no. 4971, p. 587, 1965.

[54] J. Ronald, "Quantitative X-ray diffraction analysis using clay mineral standards extracted from the samples to be analysed," *Clay Minerals*, vol. 7, no. 1, pp. 79–90, 1967.

[55] R. L. Folk, *Petrology of Sedimentary Rocks*, Hemphill, Austin, TX, 1968.

[56] Y. C. Cao, Y. Tian, M. Song et al., "Characteristics of low-permeability clastic reservoirs and genesis of relatively high-quality reservoirs in the continental rift lake basin: a case study of Paleogene in the Dongying sag, Jiyang depression," *Acta Petrolei Sinica*, vol. 39, no. 7, pp. 727–743, 2018.

[57] X. P. Yang, W. Z. Zhao, C. N. Zou, M. J. Chen, and Y. R. Guo, "Origin of low-permeability reservoir and distribution of favorable reservoir," *Acta Petrolei Sinica*, vol. 28, no. 4, pp. 57–61, 2007.

[58] J. Z. Du, J. G. Cai, Z. H. Xie, and X. J. Wang, "Chloritization sequences in mudstone during diagenesis and its geological significance," *Geological Journal of China Universities*, vol. 24, no. 1, pp. 371–379, 2018.

[59] Y. Wen, *Favorable Reservoir Genesis of Sandstone in Wenchang Formation of Lufeng Sag*, Published master dissertation, Chengdu University of Technology, Chengdu, China, 2020.

[60] S. Ehrenberg, "Preservation of anomalously high porosity in deeply buried sandstones by grain-coating chlorite: examples from the Norwegian continental shelf," *AAPG Bulletin*, vol. 77, no. 7, pp. 1260–1286, 1993.

[61] Z. Cao, C. Lin, C. Dong et al., "Impact of sequence stratigraphy, depositional facies, diagenesis and CO_2 charge on reservoir quality of the lower cretaceous Quantou Formation, Southern Songliao Basin, China," *Marine and Petroleum Geology*, vol. 93, pp. 497–519, 2018.

[62] C. Lan, M. Yang, and Y. Zhang, "Impact of sequence stratigraphy, depositional facies and diagenesis on reservoir quality: a case study on the Pennsylvanian Taiyuan sandstones, northeastern Ordos Basin, China," *Marine and Petroleum Geology*, vol. 69, pp. 216–230, 2016.

[63] A. Abu Mostafa, A. M. Abu Khadrah, and A. A. Refaat, "Impact of diagenesis on reservoir quality evolution of the late Cenomanian Abu Roash "G" Member in the Sitra Field, North Western Desert, Egypt," *Marine and Petroleum Geology*, vol. 95, pp. 255–264, 2018.

[64] S. Anjos, L. De Ros, R. Souza, C. Silva, and C. Sombra, "Depositional and diagenetic controls on the reservoir quality of Lower Cretaceous Pendência sandstones, Potiguar rift basin, Brazil," *AAPG bulletin*, vol. 84, pp. 1719–1742, 2000.

[65] A. Karim, G. Pe-Piper, and D. J. Piper, "Controls on diagenesis of Lower Cretaceous reservoir sandstones in the western Sable Subbasin, offshore Nova Scotia," *Sedimentary Geology*, vol. 224, no. 1-4, pp. 65–83, 2010.

[66] Q. M. Cao, *Formation Mechanism of Middle-Deep Sandstone Reservoir of Eocene in Zhu I Depression, Pearl River Mouth Basin*, Chengdu University of Technology, Chengdu, China, 2021.

[67] K. Bjorlykke and P. Egeberg, "Quartz cementation in sedimentary basins," *AAPG Bulletin*, vol. 77, pp. 1538–1548, 1993.

[68] R. Worden and S. Morad, "Clay minerals in sandstones: controls on formation, distribution and evolution," *Clay mineral cements in sandstones*, 2009.

[69] J. Kantorowicz, "The influence of variations in illite morphology on the permeability of Middle Jurassic Brent Group sandstones, Cormorant Field, UK North Sea," *Marine and Petroleum Geology*, vol. 7, no. 1, pp. 66–74, 1990.

[70] R. Worden and S. Morad, *Quartz Cementation in Sandstones*, 2009.

[71] R. Surdam, S. Boese, and L. Crossey, "The chemistry of secondary porosity," in *Clastic Diagenesis*, vol. 37, pp. 127–151, AAPG Memoir, 1984.

[72] R. C. Surdam, L. Crossey, E. S. Hagen, and H. Heasler, "Organic-inorganic interactions and sandstone diagenesis," *AAPG Bulletin*, vol. 73, pp. 1–23, 1989.

[73] Y. C. Cao, G. H. Yuan, X. Y. Li, T. Yang, and Y. Z. Wang, "Types and characteristics of anomalously high porosity zones in Paleogene mid-deep buried reservoirs in the northern slope, Dongying Sag," *Acta Petrolei Sinica*, vol. 34, no. 4, pp. 77–85, 2013.

[74] S. Paxton, J. O. Szabo, J. Ajdukiewicz, and R. E. Klimentidis, "Construction of an intergranular volume compaction curve for evaluating and predicting compaction and porosity loss

in rigid-grain sandstone reservoirs," *AAPG Bulletin*, vol. 86, pp. 2047–2067, 2002.

[75] A. M. E. Marchand, P. Smalley, R. S. Haszeldine, and A. E. Fallick, "Note on the importance of hydrocarbon fill for reservoir quality prediction in sandstones," *AAPG Bulletin*, vol. 86, no. 9, pp. 1561–1571, 2002.

[76] Y. D. Dai, Z. C. Niu, and X. D. Wang, "Differences of hydrocarbon enrichment regularities and their main controlling factors between Paleogene and Neogene in Lufeng sag, Pearl River Mouth Basin," *Acta Petrolei Sinica*, vol. 40, no. s1, pp. 41–52, 2019.